RSC Advances

ROYAL SOCIETY OF CHEMISTRY

www.rsc.org/advances

Journal Name

RSCPublishing

ARTICLE

Solvatochromic properties of 3,6-di-tert-butyl-8H-indolo[3,2,1-de]acridin-8-one

Cite this: DOI: 10.1039/x0xx00000x

Received ooth January 2012,
Accepted ooth January 2012

DOI: 10.1039/x0xx00000x

www.rsc.org/

Marlena Czerwińska, Małgorzata Wierzbicka, Katarzyna Guzow, Irena Bylińska, Wiesław Wiczk*

Abstract

The spectral and photophysical properties of newly synthesized 3,6-di-tert-butyl-8H-indolo[3,2,1-de]acridin-8-one were studied. To determine the contribution of specific and nonspecific interactions of this compound with solvents, the solvatochromic methods were used. It was found that bathochromic shifts of absorption and fluorescence spectra were mostly caused by polarizability/dipolarity interactions of the solute with solvent. The excited state dipole moment, determined based on solvatochromic method, is two times higher than that in the ground state. Also, the spectral and photophysical properties of compound studied correlate with E_T^N solvent polarity scale. The radiative rate constant does not depend on the solvent properties, while the non-radiative rate constant decreases with increasing solvent polarity. Such decrease of non-radiative rate constant with lowering of energy gap between S_0 and S_1 states indicates on the participation of triplet state in the deactivation of the excited state. After photoexcitation hydrogen bond energy increases in both locally excited Franck-Condon and relaxed excited state, however, the change of hydrogen bonds energy is three times higher in the relaxed excited state. The hydrogen bond energy change measured in five alcohols correlates with the Kamlet-Taft or Catalán solvent acidity parameter.

Journal Name RSCPublishing

ARTICLE

1 Introduction

It is well known that natural and synthetic acridines/acridones possesses antitumor activity[1-3] and DNA photo-damaging ability[4]. Their biological activity is mainly attributed to the planarity of these aromatic compounds, which enables intercalation within the double-stranded DNA structure, thus interfering with the cellular machinery. Besides biological activity, acridone and its derivatives exhibit a high fluorescence quantum yield and characterized by a high photostability. For this reason, are used, among others, as a sensor for fluorescence detection of DNA[5-8]. Studied compound 3,6-di-tert-butyl-8H-indolo[3,2,1-de]acridin-8-one belongs to the acridone group comprising many potential drugs or fluorescent probe. To determine whether it is suitable as a fluorescent sensor the factors influencing photophysical properties should be determined. To establish what type of interactions are important ones in the solute-solvent interactions, we performed a detailed study of the environmental impact on spectral and photophysical properties of 3,6-di-tert-butyl-8H-indolo[3,2,1-de]acridin-8-one.

It is commonly acknowledged that solvent-dependent UV–Vis spectral band shifts can arise from either general and/or specific solvent effects[9]. The first effect results from isotropic interactions of the chromophore dipole moment with the reaction field induced in the surrounding solvent. Specific effects result from the short-range anisotropic interactions between the chromophore with one or more solvent molecules in its first solvation shell, an important example of which is the formation of hydrogen bonds. It is thus of interest to quantify the relative contributions from these two effects[10,11]. The electronic transition in molecules, involving intramolecular charge transfer, is very sensitive to the nature of the microenvironment around the solute and the spectral parameters can be used to study solute-solvent interactions at the microscopic level[12-15]. In the case of different electron densities in the electronic ground and excited state of a light-absorbing molecule, its dipole moment varies in these two states. Thus, a change of the solvent affects the ground and excited state differently. The solvent-dependent photophysical characteristic can be investigated by steady-state absorption and emission spectroscopy as well as time-resolved fluorimetry. From these experiments, the position of the spectra maxima, the Stokes shift, fluorescence lifetime and the rate constants of radiative and non-radiative deactivation of compound studied are determined[12-15]. The normalized E_T^N polarity scale[16,17], Bilot-Kawski solvent polarizability functions[18-21], and Kamlet-Taft[22] and Catalán[23] multi-parameters solvent scales are used to describe the solvent effect on the spectral and photophysical properties. The changes of the hydrogen bond after excitation are also addressed[10,24-28]. In this work, applying the solvatochromic methods the influence of solvents on the spectral and photophysical properties and hydrogen bond energy changes after photoexcitation as well as multi-linear correlations of newly synthesized 3,6-di-tert-butyl-8H-indolo[3,2,1-de]acridin-8-one (**3**, Fig. 1), are presented.

2 Experimental

2.1 Synthesis

Synthesis of 3,6-di-tert-butyl-8H-indolo[3,2,1-de]acridin-8-one was performed according to the scheme (Fig. 1).

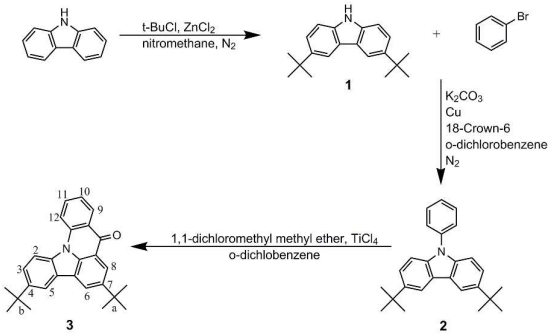

Fig. 1 Scheme of 3,6-di-tert-butyl-8H-indolo[3,2,1-de]acridin-8-one synthesis.

To obtain 3,6-di-tert-butyl-9*H*-carbazole (compound 1) and 9-phenyl-3,6-di-tert-butyl-9*H*-carbazole (compound 2) literature procedures were applied[29]. Both compounds were purified by column chromatography (Merck, Silica gel 60, 0.040-0.063 mm, eluent: CH_2Cl_2:petroleum ether 1:10 (v/v) (compound 1), CH_2Cl_2:petroleum ether 1:5 (v/v) (compound 2)) and then crystallized from boiling petroleum ether. Compound 1 was obtained with 46% yield whereas compound 2 with 29% yield. The title compound **3** was obtained applying procedure described in[30]. To a stirred solution of 9-phenyl-3,6-di-tert-butyl-9*H*-carbazole (compound **2**) (0.09 g, 0.253 mmol) in 1,2-dichlorobenzene (5 ml) cooled in an ice bath, 1,1-dichloromethyl methyl ether (0.033 ml, 0.365 mmol) and $TiCl_4$ (0.046 ml, 0.419 mmol) were added. The reaction was continued for 1 hour in the ice bath. Then the reaction mixture was allowed to warm up to the room temperature and poured on ice (14.05 g) and concentrated HCl (0.63 ml). The organic layer was diluted with chloroform, washed with a 5% solution of HCl (1x) and water (3x) and dried with anhydrous Na_2SO_4. After evaporation the residue (yellow solid) was purified by column chromatography (Merck, Silica gel 60, 0.040–0.063 mm) using a mixture of CH_2Cl_2:petroleum ether 1:2 (v/v) as an eluent. Additional purification was performed using RP-HPLC (Kromasil column, C-8, 5 µm, 250 mm long, i.d.=20 mm; linear gradient 50-100%B over 120 minutes, A=0.1% water solution of trifluoroacetic acid, B=80% of acetonitrile in A) giving desired compound as a yellowish-orange solid (0.064 g, 0.168 mmol, 66% yield). The purity of the obtained compound was checked by RP-HPLC using analytical column Phenomenex Jupiter® (C-18, 5 µm, 250 mm long, i.d.=4.6 mm, gradient 50-100% B over 30 minutes, λ=223 nm, 245 nm, 300 nm, t_R=28.3 min.). The product was identified by means of the ^{1}H and ^{1}H-^{1}H COSY NMR (Bruker AVANCE III spectrometer (500 MHz) in $CDCl_3$), IR spectrum (Bruker IFS-66 instrument) and mass spectrum (Bruker Biflex III (MALDI-TOF)). m.p. 237-241 °C; MS: m/z=382.2 $(M+H)^+$; IR (KBr): ν_{max} (cm^{-1}) 2867.7-2953.9 CH; 1648.0 C=O; 1442.6-1484.0 C=C; 1144.6-1264.4 $C(CH_3)_3$; ^{1}H NMR: δ (ppm) 1.537 (s, 9H, $(CH_3)_3$ (a)); 1.581 (s, 9H, $(CH_3)_3$ (b)); 7.497-7.529 (m, 1H, $C^{11}H$); 7.714 (dd, 1H, C^3H, J=2.0 Hz, J=8.8 Hz); 7.920-7.955 (m, 1H, $C^{10}H$); 8.247-8.264 (m, 2H, C^2H, C^8H); 8.495 (d, 1H, C^9H, J=8.5 Hz); 8.532 (d, 1H, C^5H, J=2.0 Hz), 8.551 (d, 1H, C^6H, J=2.0 Hz); 8.757 (dd, 1H, $C^{12}H$, J=1.5 Hz, J=8.0 Hz). In 2D NMR ^{1}H-^{1}H COSY spectrum the following correlation signals were observed: the coupling of $C^{11}H$ (δ=7.5 ppm) with $C^{10}H$ (δ=7.9 ppm) and $C^{12}H$ (δ=8.8 ppm), the coupling of $C^{10}H$ (δ=7.9 ppm) with

C^9H (δ=8.5 ppm), the coupling of C^3H (δ=7.7 ppm) with C^2H (δ=8.2 ppm). For hydrogen atoms C^5H, C^6H and C^8H no correlation signals were observed indicating on the absence of their coupling with other hydrogen atoms present in the molecule.

2.2 Spectroscopic measurements

The UV/Vis absorption spectra in all 26 solvents studied were measured using a Perkin-Elmer Lambda 40P spectrophotometer, whereas emission spectra were measured using a Horiba-Jobin Yvon FluoroMax-4 spectrofluorimeter. Solvents of the highest available quality were used. Fluorescence quantum yields (Φ) were calculated with quinine sulphate in 0.5 M H_2SO_4 (Φ= 0.53 ± 0.02) as reference and were corrected for different refractive indices of solvents[31]. In all fluorimetric measurements, the optical density of the solution does not exceed 0.1. Luminescence spectra were measured in quartz capillaries at liquid nitrogen temperature using a low-temperature accessory. The fluorescence lifetimes were measured with a time-correlated single-photon counting apparatus Edinburgh CD-900 equipped with NanoLed N16 (UV LED λ=339 nm) from IBH as the excitation source. The half-width of the response function of the apparatus, measured using a Ludox solution as a scatter, was about 1.0 ns. The emission wavelengths were isolated using a monochromator. Fluorescence decay data were fitted by the iterative convolution to the sum of exponents according to eq.:

$$I(t) = \sum_i \alpha_i \exp(-t/\tau_i) \quad (1)$$

where α_i is the pre-exponential factor obtained from the fluorescence intensity decay analysis and τ_i the decay time of the i-th component, using a software supported by the manufacturer. The adequacy of the exponential decay fitting was judged by visual inspection of the plots of weighted residuals as well as by the statistical parameter χ^2_R and shape of the autocorrelation function of the weighted residuals and serial variance ratio (SVR).
Linear and multi-parametric correlations were performed using Origin v. 9 software.

3 Results and discussion

3.1 Spectral properties

Absorption spectra of the title compound in selected solvents are presented in Fig. 2, whereas the emission spectra in Fig. 3.

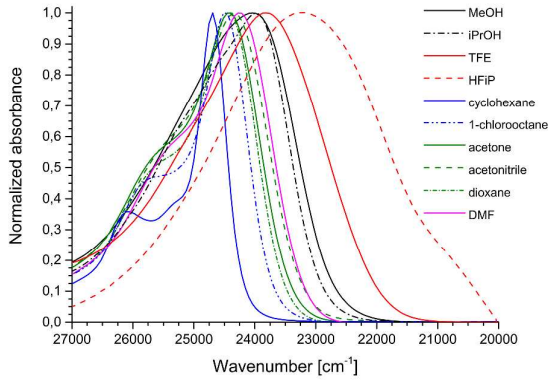

Fig. 2 Absorption spectra of 3,6-di-tert-butyl-8H-indolo[3,2,1-de]acridin-8-one in selected solvents.

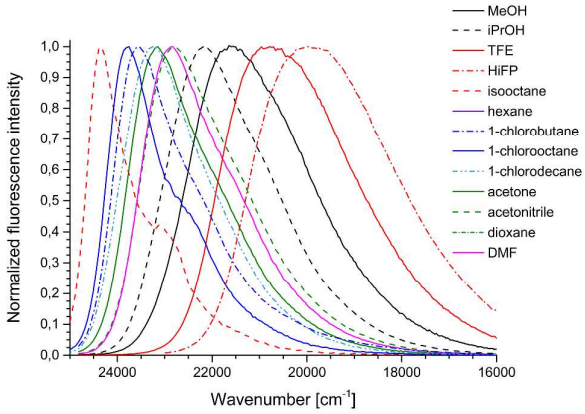

Fig. 3 Emission spectra of 3,6-di-tert-butyl-8H-indolo[3,2,1-de]acridin-8-one in selected solvents.

In non-polar solvents, saturated hydrocarbons and 1-chloroalkanes, absorption spectrum possesses a maximum at about 24700 cm^{-1}. The spectra in these solvents have small half-width and the most intense is the first vibronic band with poorly separated vibrational structure on the short-wavelength side of the spectrum. The increase of solvent polarity causes bathochromic shift of the spectrum and the simultaneous loss of the vibrational structure. In protic solvent, the long-wavelength absorption band takes bell shape form and the position of its maximum shifts with increasing proton-donor capacity of the solvent. However, the bathochromic shift of the absorption band is not substantial and ranges from 24690 cm^{-1} for cyclohexane to 24100 cm^{-1} in MeOH. A larger bathochromic shift is observed for TFE (2,2,2-trifluoroethanol) (23700 cm^{-1}) and HFIP (1,1,1,3,3,3-hexafluoro-2-propanol) (22990 cm^{-1}).

More substantial changes are observed in emission spectra (Fig. 3). In non-polar solvents the emission spectra possess a maximum at about 24100 cm^{-1} with weakly marked vibrational structure. An increase of solvent polarity results in bathochromic shift of the spectrum and loss of its vibrational structure. Like for absorption spectra, a major bathochromic shift of emission band is observed in alcohols. The larger proton-donor properties of alcohol, the greater shift is observed (position of the emission band maximum is located at 22200 cm^{-1} for 2–propanol whereas at 19800 $cm^{-1}$for HFIP). The spectral and photophysical properties of compound studied are gathered in Table 1.

Solvent properties influences fluorescence quantum yield and fluorescence lifetime of the studied compound (Table 1). Larger fluorescence quantum yields are observed in alcohols (up to 0.69 for HFIP) and polar solvents whereas for non-polar solvents these values are relatively small (about 0.01 for hexane). Similarly, fluorescence lifetimes are longer for protic and polar solvents (about 6.7 ns for HFIP) and much shorter for non-polar solvents (0.98 ns for hexane). It should be noted that in all solvents studied the fluorescence intensity decay is mono-exponential, except ethyl ether in which fluorescence intensity decay of 3,6-di-tert-butyl-8H-indolo[3,2,1-de]acridin-8-one is bi-exponential indicating on its specific interaction with this solvent.

3.2 Correlation with Reichardt's E_T^N solvent polarity scale parameter

The various models of solvation, several empirical solvent polarity parameters have been proposed to characterize and rank empirically the polarity of a solvent[16,17,22,23]. One of the most popular solvent polarity scale is the $E_T(30)$ scale, based on Vis spectroscopic band shifts of a negatively solvatochromic

standard probe[16,17], or the normalized E_T^N parameter defined according to equation (2):

$$E_T^N = \frac{E_T(solvent) - E_T(TMS)}{E_T(water) - E_T(TMS)} \quad (2)$$

where TMS denotes tetramethylsilane. They are mostly used to correlate the absorption or emission transition energies and Stokes shifts[13-15,32,33].

As mentioned above, the maxima of absorption spectra shift to the red with increasing solvent polarity. The plot of dependence of wavenumber of maximum of absorption spectrum *versus* E_T^N (Fig. 1 ESI) reveals rather week correlation (r^2=0.8812, N=21). Main reason for the lack of good correlation is large deviations observed for alcohols, especially for TFE and HFIP, but also for other solvents such as toluene or DMSO. This indicates on a specific solute-solvent interactions. Separate analyses of the data for the protic and non-protic solvents do not improve the correlation. For non-protic solvents correlation coefficient is r^2=0.7349 for 16 solvents whereas for protic ones r^2=0.6745 (N=5) (Fig. 1 ESI). A better correlation with Reichardt`s solvent polarity parameter (E_T^N) (r^2=0.9554, N=21) was obtained for the position of emission maximum (Fig. 2 ESI). However, the experimental points for non-protic solvents are grouped in three clusters of points which give bad correlation coefficient (r^2=0.7645, N=16) with E_T^N, in opposite to protic solvents (r^2=0.9823, N=5). The Stokes shift correlates well with the E_T^N parameter after the rejection of the points corresponding to ethyl ether and DMSO, (r^2=0.9829, N=19) and there is no reason to analyse separately protic and non-protic solvents (Fig. 3 ESI). Also, the dependence of fluorescence quantum yield on E_T^N parameter does not give rise to a division of solvents into two groups, however, the correlation coefficient is rather small (r^2=0.8848, N=21) due to the large deviation from a straight line observed for polar solvents (Fig. 4 ESI). The dependence of fluorescence lifetime can be described as a straight-line dependence on E_T^N parameter with good correlation coefficient (r^2=0.9594, N=20, Fig. 5 ESI). However, it can be seen that the fluorescence decay time values measured in alcohols clearly differ in a systematic way from this relationship. A separate analysis of fluorescence lifetime dependence on E_T^N for protic and non-protic solvents (Fig. 5 ESI) gave a worse value of correlation coefficient for non-protic solvents (r^2=0.8858, N=15), however, a better correlation for protic solvents (r^2=0.9817, N=5).

Both fluorescence quantum yield and fluorescence lifetime are complex function of fluorescence and non-radiative rate constant. For the mono-exponential fluorescence intensity decay, the radiative (k_f) and non-radiative (k_{nr}) rate constants can be calculated from the measured fluorescence quantum yield (Φ) and fluorescence lifetime (τ) according to equations (3) and (4):

$$k_f = \Phi / \tau \quad (3)$$

$$k_{nr} = (1 - \Phi) / \tau \quad (4)$$

Therefore, an analysis of these rate constants as a function of E_T^N was performed to receive information which of them and how depend on the solvent parameters, enabling to estimate which path of the excited state deactivation predominates.

It was found that the radiative rate constant (k_f) poorly depends on E_T^N (r^2=0.2319, N=15) (Fig. 6 ESI) even after exclusion of the data corresponding to hydrocarbon solvents. Very large deviation from correlation line of k_f values in hydrocarbon solvents may indicate that in these solvents the fluorescence occurs from a different state than in the other ones.

In the case of dependence of non-radiative rate constant (k_{nr}) on E_T^N parameter, separate analyses for the protic and non-protic solvents have to be performed (Fig. 7 ESI). In both cases, the increase of solvent polarity causes a decrease of non-radiative rate constant as indicated by negative slope –(3.63±0.27), (r^2=0.9334, N=15) for non-protic solvents and -(1.89±0.19), (r^2=0.9695, N=5) for protic ones. Thus, the solute-solvent interactions with polar environment decrease the non-radiative rate constant of 3,6-di-tert-butyl-8H-indolo[3,2,1-de]acridin-8-one. Moreover, this process is slower in alcohols than in non-protic solvents. The strong increase of k_{nr} upon solvent polarity can be rationalized if k_{nr} can be attributed mainly to internal conversion (the energy gap lowering)[15,29]. In the opposite case, the main path of the excited state deactivation is intersystem crossing to the triplet state[30].

According to Englman and Jortner[34] the weak coupling limit (the relative horizontal displacement of the two potential energy surfaces is small) reveals an exponential dependence of the transition probability on the energy gap ΔE. The dependence of non-radiative rate constant on the energy gap between two electronic states can be roughly estimated from equation[35]:

$$\log(k_{IC}) \approx 12 - 2\nu_{fluo}^{max} \quad (5)$$

where: k_{IC} is the rate constant of internal conversion expressed in s^{-1} and ν_{fluo}^{max} expressed in μm^{-1}. As can be seen from the formula (5) the bathochromic shift of fluorescence spectrum causes the increase of the non-radiative rate constant. In the case studied, a bathochromic shift of emission spectra is observed with increase of solvent polarity, however, the decrease of the non-radiative rate constant is recorded. An inverse relationship between non-radiative rate constant (k_{nr}) and the environment polarity and thereby decreasing the energy gap between relaxed excited state and ground state (Fig. 4) is in opposition to that founded in literature[15,29]. The plot of ln(k_{nr}) as a function of energy gap between S_1 and S_0 states ($\Delta E(S_1\text{-}S_0) = \nu_{fluo}^{max}$) gives two straight lines (Fig. 4).

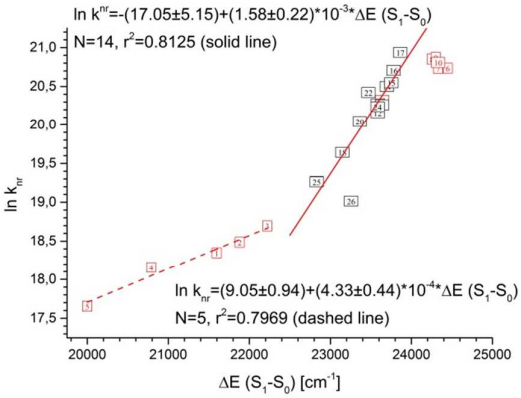

Fig. 4 Correlations between the logarithm of the non-radiative rate constant ln(k_{nr}) and $\Delta E(S_1\text{-}S_0) = \nu_{fluo}^{max}$ energy gap for 3,6-di-tert-butyl-8H-indolo[3,2,1-de]acridin-8-one in studied solvents.

A slope is equal to (1.58±0.22)*10^{-3}, (r^2=0.8125, N=15, without hydrocarbon solvents which form a separate cluster of points) for non-protic solvents and (4.33±0.44)*10^{-4}, (r^2=0.7969, N=5) for protic ones.

To further investigate the dependence of non-radiative rate constant on solvent polarity, luminescence spectra of studied compound were measured in several solvents. In non-polar methylcyclohexane (MeCx), apart from weak fluorescence

spectrum shifted to the red compared to the spectrum measured at room temperature, a strong phosphorescence spectrum is observed (Fig. 8 ESI). This indicates that the main deactivation route of the excited state is the intersystem crossing to the triplet state, hence, low fluorescence quantum yield and short fluorescence lifetime observed in saturated hydrocarbon solvents. The situation is different in protic solvents. In methanol glass only weak phosphorescence is visible as a shoulder on the red-side of the fluorescence spectrum (Fig. 9 ESI). In a weakly polar and polar solvents (MeTHF, C_3H_7Cl, DMF) well separated fluorescence and phosphorescence spectra are observed (Fig. 5, Fig. 10 ESI).

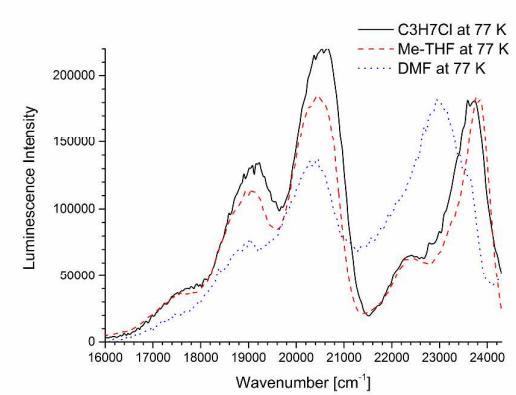

Fig. 5 The luminescence spectra of 3,6-di-tert-butyl-8H-indolo[3,2,1-de]acridin-8-one (normalized to the same fluorescence intensity) in C_3H_7Cl, MeTHF and DMF measured at 77 K.

It is worth mentioning that the phosphorescence spectrum with maximum at 20400 cm^{-1} and well-resolved vibrational structure practically does not depend on solvent polarity, contrary to the fluorescence spectrum. Additionally, the ratio of phosphorescence to fluorescence intensity decreases with an increase of solvent polarity (Fig. 5). To explain such a relationship the interdependence of the internal conversion and intersystem crossing rate constants should be examined. Radiationless rate constant (k_{nr}) is the sum of internal conversion (k_{IC}) and intersystem crossing (k_{ISC}) rate constants. The observed decrease of k_{nr} with decrease of (S_1-S_0) energy gap can be rationalized assuming decrease of intersystem rate constant. One can assume that the excited state lies over two (n,π^*) and ($\pi\pi^*$) states. Two scenarios are possible. In the first one, a decrease of the energy gap between S_1 and S_0 states at the same time lowers the energy of $S_1(\pi\pi^*)$ state below the $T(n,\pi^*)$ state so that it is located between triplet states. According to El-Sayed rule[36], the rate constant of intersystem crossing (k_{ISC}) is greater for $S_1(\pi\pi^*)\rightarrow T(n,\pi^*)$ than for $S_1(\pi\pi^*)\rightarrow T(\pi\pi^*)$ transition. Thus, as a result of the decrease of the energy of excited singlet, the intersystem crossing between $S_1(\pi\pi^*)\rightarrow T(\pi\pi^*)$ state takes place resulting in the decrease of intersystem rate constant and therefore an increase in the fluorescence intensity and decrease in the phosphorescence intensity is observed. Based on such a mechanism the differences in the photophysics of 2-nitrofluorene with that of 2-diethylamino-7-nitrofluorene was explained[37]. A second possible mechanism may result from the reduction of Franck-Condon factor in the $S_1\rightarrow T_1$ intersystem crossing process which is the result of the increase of the ICT participation in the S_1 state (Fig. 11 ESI). In both of these explanation one assumes no effect or little effect of the solvent polarity on the internal conversion rate constant. Based on collected data, the second mechanism seems to be more probable.

Thus, it seems that efficient intersystem crossing to a triplet state determines photophysical properties of 3,6-di-tert-butyl-8H-indolo[3,2,1-de]acridin-8-one (low fluorescence quantum yield and short fluorescence lifetime) in non-polar and weakly polar solvents.

3.3 Multi-parametric correlations

The multiple linear regression, approach of Kamlet and coworkers[22] and Catalán[23], has been used to correlate UV–Vis absorption and emission energies[14,15,38] as well as another photophysical properties with an index of the solvent dipolarity/polarizability which is a measure of the solvent's ability to stabilize a charge or dipole through nonspecific dielectric interactions (π* or SP and solvent dipolarity SdP in a new generalized solvent polarity Catalán scale), and indices of the solvent's hydrogen-bond donor strength (α or SA) and hydrogen-bond acceptor strength (β or SB) according to eqs: (6) and (7):

$$y = y_0 + a_{\pi^*}\cdot\pi + b_{\alpha}\cdot\alpha + c_{\beta}\cdot\beta \qquad (6)$$

or

$$y = y_0 + a_{SP}\cdot SP + b_{SdP}\cdot SdP + c_{SA}\cdot SA + d_{SB}\cdot SB \quad (7)$$

where: y denotes a solvent-dependent physicochemical property in a given solvent and y_0 the statistical quantity corresponding to the value of the property in the gas phase; π^*, α, β, SP, SdP, SA, SB represent independent solvent parameters accounting for various types of solute–solvent interactions; a_{π^*}, b_{α}, c_{β} and a_{SP}, b_{SdP}, c_{SA} and d_{SB} are adjustable coefficients that reflect the sensitivity of physical property y in a given solvent to the various solvent parameters.

The results of multi-linear correlation according to Catalán and Kamlet-Taft equations are presented in Tables 2 and 3. Both solvent polarity scales predict a bathochromic shift of absorption spectra with increase of solvent polarity (all coefficients in Eqs (6) and (7) are negative). A fair fit was obtained in both cases (r^2=0.9190 for Catalán and r^2=0.9231 for Kamlet-Taft correlation, respectively). In the Catalán equation all four coefficients are important. However, the large values of a_{SP} (51.5%) and d_{SA} (33%) coefficients compared to the others indicate that the changes of ν_{abs} may reflect primarily a change in polarizability and acidity of the environment of the chromophore, whereas the solvent dipolarity (9%) and basicity (6.5%) have a minor influence. The same conclusion can be drown from Kamlet-Taft correlation. Two parameters, solvent dipolarity/polarizability (π^*) and solvent acidity (α), influenced equally (in about 50%) the bathochromic shift of absorption spectra, while solvent basicity can be omitted because of low value and large error exceeding the value of the parameter (the quality of fit decrease a little to r^2=0.9139 comparing to the original fir r^2=0.9231). Good quality of fits were obtained in multi-linear correlations of the position of fluorescence maximum (r^2=0.9510 for Catalán and r^2=0.9731 for Kamlet-Taft correlation). In both cases, solvent basicity has minor influence on bathochromic shift of fluorescence spectrum ($c_{SB}\approx$ 12%), whereas the solvent acidity ($d_{SA}\approx$74%) and solvent dipolarity ($b_{SdP}\approx$26%) have major influence on it. Solvent polarizability in the Catalán equation may be disregarded because of its large error without substantial decrease of the quality of fit (r^2=0.9500 compared to the original fit r^2=0.9510). A similar results were obtained from Kamlet-Taft correlation (r^2=0.9731). A bathochromic shift of fluorescence spectrum is caused mainly by solvent dipolarity/polarizability (35%) and solvent acidity (55%), while solvent basicity has a minor influence (10%). It is worth mentioning that the correlation parameters for both absorption and emission spectra are negative meaning that their changes cause red-shift of the spectra. Additionally, correlation parameters obtained for fluorescence spectra are larger, taking into account their absolute values, than those calculated for absorption spectra. This indicates that the electronic structure of the locally excited Franck-Condon and relaxed excited states of 3,6-di-tert-butyl-

8H-indolo[3,2,1-de]acridin-8-one differ significantly, and the relaxed excited state is more polar.

Correlation of the Stokes shift with the four-parameter solvent scale (r^2=0.9311) reveals that the increase of solvent polarizability decreases the Stokes shift (a negative value of adjustment parameter) in opposite to the remaining three parameters. The biggest contributions to the changes of Stokes shift have solvent polarizability (41%) and solvent acidity (37%), whereas the solvent dipolarity (15%) and solvent basicity (7%) have minor influence on a Stokes shift. A good correlation of the Stokes shift was also obtained using Kamlet-Taft equation (r^2=0.9241). In this case, two parameters, solvent polarizability/polarity (41%) and solvent acidity (59%), play a crucial role. Because of a small value and large error, solvent basicity can be omitted without deterioration of the quality of fit (r^2=0.9160 whereas for original fit r^2=0.9241).

The correlation of the fluorescence quantum yield with SP, SdP, SA, SB as independent variables gives a rather good fit (r^2=0.8879, Table 2). Moreover, it indicates that all solvent parameters influence the fluorescence quantum yield. Solvent acidity (37%) and solvent dipolarity (42%) increases the fluorescence quantum yield to a similar degree, while solvent dipolarity and basicity have only a little impact on it (9% and 12%, respectively). The same conclusion arises from the Kamlet-Taft correlation (r^2=0.9306). Solvent polarizability/dipolarity and solvent acidity affect almost equally (42% and 41%, respectively) while solvent basicity in a much lesser extent (17%).

A good fit was also obtained for the fluorescence lifetime correlation with both Catalán (r^2=0.9386) and Kamlet-Taft (r^2=0.9638) equations. The largest impact on the increase of fluorescence lifetime has solvent acidity (68% and 53% for Catalán and Kamlet-Taft correlation, respectively) whereas solvent dipolarity contributes with 14% and 17%, respectively. Moreover, the contribution of solvent basicity is different for these two solvent scale. For Kamlet-Taft scale solvent basicity contribution (30%) is almost twice of that of Catalán scale (18%).

The decay of the fluorescence intensity of 3,6-di-tert-butyl-8H-indolo[3,2,1-de]acridin-8-one can be described as a mono-exponential function, except for ethyl ether solution, thus, further analysis including the dependence of fluorescence lifetime, fluorescence rate constant and radiationless rate constant on solvent polarity parameters can be performed. Analysis of the influence of the solvent on the radiative and non-radiative rate constants gives information which one depends on the solvent parameters enabling to estimate which path of the excited state deactivation predominates. The multi-linear analysis of k_f according to eq. (6) and (7) revealed that it does not correlate with solvent parameters (r^2=0.4389 for Catalán and r^2=0.4070 for Kamlet-Taft correlation, respectively) (Tables 2 and 3), however, it depends exclusively on solvent polarizability/polarity. In contrast to k_f, non-radiative rate constant k_{nr} give good correlations (r^2=0.8987 for Catalán and r^2=0.9441 for Kamlet-Taft equation, respectively) with all adjustment coefficients negative. The larger decrease of k_{nr} is caused by solvent polarizability/polarity (44% and 50% for Catalán and Kamlet-Taft correlation, respectively), solvent acidity (36% and 23%) and solvent basicity (20% and 27%). It is worth mentioning that solvent polarizability in Catalán solvent scale has no impact on k_{nr}. Moreover, a good correlation between k_{nr} and solvent acidity parameter (α and SA) for alcohols were found (Figs 12 ESI and 13 ESI). Thus, the invariance of k_f and dependence of k_{nr} on the solvent properties indicate that the change of the fluorescence quantum yield and the fluorescence decay time with solvent properties is mainly due to the change of the k_{nr} rate constant.

Among three different solvent polarity scales used in this work, Reichardt`s empirical one is a useful and easy to apply, but because it is a one-parameter scale, it does not reflect the complexity of solute-solvent interactions. However, it allows to easily determine whether the solvent studied shows a deviation from linearity due to specific interactions. Its additional advantage is possibility to estimate the dipole moment change in the excited state based on the Stokes shift dependence on E_T^N. Another two solvent polarity scales are more useful as they are multi-parametric. They allow to estimate the impact of various solvent parameters on studied quantity. For this reason a four-parameter scale has advantage over the Kamlet-Taft scale because it allows to assess independently the impact of both the polarizability and dipolarity, however, both offer comparable quality of the fit. In the case of multi-parametric solvents scales, better quality of the fits are obtained than for Reichardt`s due to the greater number of variables. Thus, in order to evaluate which scale used gives a better quality of the fit, the adjusted r^2 rather than coefficient of determination (r^2) should be applied. The explanation of adjusted r^2 is almost the same as r^2 but it penalizes the statistics as extra variables included in the model.

3.4 Specific interactions

A variety of solvent interactions with solute may be responsible for the solvent effect on the properties of solute. The solvent effect can be split into two different type of interactions: specific involving charge-transfer interactions, acid-base interactions, π-π interactions and hydrogen bonding, while those interactions which arise from the solvent acting as a dielectric continuum are referred to as non-specific interactions. The classification of solvents with respect to their polarity/polarizability and hydrogen bonding ability are based on the Kamlet-Taft or Catalán solvent polarity scale. Solvents capable to form hydrogen bond have been classified as hydrogen-bond acceptors, e.g. possessing ability to accept hydrogen atom from solute (β parameter in Kamlet-Taft scale or SB parameter in Catalán scale), and hydrogen-bond donor, e.g. possessing ability to donate hydrogen atom to solute to form hydrogen bond (α parameter in Kamlet-Taft scale or SA parameter in Catalán scale). The protic solvents mostly used in solvatochromic studies have both hydrogen-donor and hydrogen-acceptor properties. In solvatochromic studies, the shift of maximum of absorption or emission spectra depends on both non-specific interactions and solute-solvent hydrogen-bonds formation.

In a series of publications, Maciejewski and co-workers[10,25-27] gave a method to extract the contribution of specific interactions between solute and hydrogen-bonding solvents based on solvatochromic data. The first step in this method requires determination of the contribution of non-specific interactions based on solvatochromic shift of absorption and emission spectra of compound studied. The solvent used for the estimation of non-specific interactions are 1-chloro-n-alkanes[10]. These solvents interact only non-specifically because they do not have π-electron, and charge-transfer character, and do not form hydrogen bond. The straight-line obtained from solvatochromic studies of solute in 1-chloro-n-alkanes describes the effect of non-specific interactions on position of maximum of absorption and emission spectra not only in these solvents but also in other solvents that make hydrogen bond. The distance between ν_{abs} or ν_{fluo} value and the straight line describes the changes in the energy of hydrogen bond in Franck-Condon excited state (from ν_{abs} dependence) or relaxed excited state (from ν_{fluo} dependence) in a given solvent according to equation (eq. 8)[10]:

$$\Delta\nu_{shift}^{abs}(H-bond)=\nu_{abs}^{\max}(f(\varepsilon,n^2))-\nu_{abs}^{\max}(\exp)$$
$$\Delta\nu_{shift}^{fluo}(H-bond)=\nu_{fluot}^{\max}(f(\varepsilon,n^2))-\nu_{fluo}^{\max}(\exp) \quad (8)$$

where: $\nu_{abs}^{\max}(\exp)$ and $\nu_{fluo}^{\max}(\exp)$ are experimental positions of the maxima of absorption and fluorescence spectra of the solute in the solvent forming the hydrogen bond, $\nu_{abs}^{\max}(f(\varepsilon,n^2))$ and $\nu_{fluo}^{\max}(f(\varepsilon,n^2))$ are the values of predicted maxima of absorption and fluorescence spectra of the solute in this solvent based on the non-specific interaction only (from straight line of solvatochromic plot) and $f(\varepsilon,n^2)$ is the orientation polarizability function. The orientation polarizability function for a spherical cavity radius can be calculated according to various formulas[11]. For a linear Stark effect and neglecting solute polarizability ($\alpha=0$) the MacRae function is used (eq. 9):

$$f_{MR}(\varepsilon,n^2)=\frac{\varepsilon-1}{\varepsilon+2}-\frac{n^2-1}{n^2+2} \quad (9)$$

Solvent polarizability function for spherical cavity with the radius (a) obtained from Bilot-Kawski theory in which linear and quadratic Stark effect was taken into account and with approximation that the polarizability of the solute is equal $2\alpha/4\pi\varepsilon_0 a^3=1$ is as follows:

$$f_{BK}(\varepsilon,n^2)=\frac{2n^2+1}{n^2+2}\left(\frac{\varepsilon-1}{\varepsilon+2}-\frac{n^2-1}{n^2+2}\right) \quad (10)$$

If the polarizability of the solute is neglected ($\alpha=0$), Lippert-Mataga in the form below is used:

$$f_{LM}(\varepsilon,n^2)=\frac{\varepsilon-1}{2\varepsilon+1}-\frac{n^2-1}{2n^2+1} \quad (11)$$

In the papers published by Maciejewski et al.[10,25-27] dedicated to the calculation of energy changes of hydrogen bonds in the excited state, the Lippert-Mataga polarizability function was used. We decided to use the Bilot-Kawski polarizability function. It is worth noting that the function selection has practically no effect on the calculated values of the hydrogen bond energy changes, however, Bilot-Kawski function has a wider range of changes, which allows a more accurate approximation of nonspecific interactions by a linear approximation. The calculated changes of energy of hydrogen bond after excitation to excited (locally excited Franck-Condon and relaxed) state of 3,6-di-tert-butyl-8H-indolo[3,2,1-de]acridin-8-one in five used alcohols are presented in Table 4 and Figs 6 and 7. As can be seen from aforementioned figures a good correlation were obtained for the dependence of $\nu_{abs}^{\max}$ and $\nu_{fluo}^{\max}$ *versus* solvent polarizability function. The low value of the slop of $\nu_{abs}^{\max}$ *vs.* $f_{BK}(\varepsilon,n^2)$ indicates that the dipole moment of compound studied is nearly the same in S_0 and S_1^{FC} state, however, in the relaxed excited state the dipole moment increases (higher negative slope of the dependence of $\nu_{fluo}^{\max}$ *vs.* $f_{BK}(\varepsilon,n^2)$). Also, like for coumarins[24], blue shift is observed for saturated hydrocarbons in both absorption and emission spectra. The deviation of these points from the line formed by 1-chloro-n-alkanes corresponds to the energy of interactions between permanent dipole moment of 1-chloro-n-alkane solvents and permanent and induced dipole moment of 3,6-di-tert-butyl-8H-indolo[3,2,1-de]acridin-8-one, while saturated hydrocarbon solvents can interact only through dispersion interaction[26].

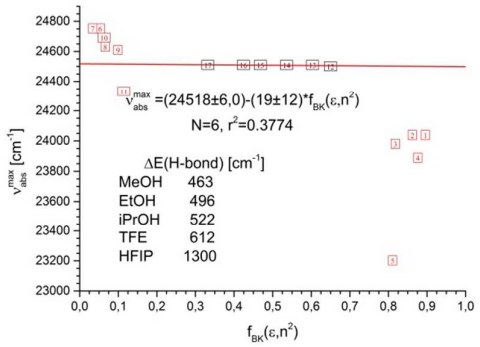

Fig. 6 The solvatochromic plot of the $\nu_{abs}^{\max}$ dependence on Bilot-Kawski polarizability function $f_{BK}(\varepsilon,n^2)$ in: (1) MeOH, (2) EtOH, (3) iPrOH, (4) TFE, (5) HFIP, (6) hexane, (7) iso-octane, (8) hexadecane, (9) squalene, (10) cyclohexane, (11) toluene (12) 1-chloro-propane, (13) 1-chloro-butane, (14) 1-chlorohexane, (15) 1-chloro-octane, (16) 1-chloro-decane, (17) 1-chlorohexadecane. The correlation equation as well as the hydrogen bond energy changes in locally excited Franck-Condon state for alcohols studied are also shown.

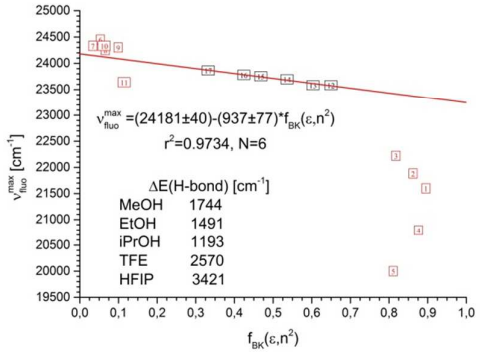

Fig. 7 The solvatochromic plot of the $\nu_{fluo}^{\max}$ dependence on Bilot-Kawski polarizability function $f_{BK}(\varepsilon,n^2)$ in: (1) MeOH, (2) EtOH, (3) iPrOH, (4) TFE, (5) HFIP, (6) hexane, (7) iso-octane, (8) hexadecane, (9) squalene, (10) cyclohexane, (11) toluene (12) 1-chloro-propane, (13) 1-chloro-butane, (14) 1-chlorohexane, (15) 1-chloro-octane, (16) 1-chloro-decane, (17) 1-chlorohexadecane. The correlation equation as well as the hydrogen bond energy changes in relaxed excited state for alcohols studied are also shown.

Moreover, red shift of absorption and emission spectrum observed for toluene can results from interactions with permanent dipole moment of solvent, however, the staking interaction with solute cannot be excluded. Because of that, in the correlation of spectroscopic properties with solvent polarizability function only 1-chloro-n-alkanes were taken into account. Moreover, the maxima of absorption and fluorescence spectra measured in alcohols are below the line defined by 1-chloro-n-alkanes which determines the non-specific interactions. Thus, the energy of hydrogen bond increases in the excited state in such a way that in the relaxed excited state the hydrogen bond is about three times stronger than that in the

locally excited Franck-Condon state (Table 4). Additionally, the changes of hydrogen bond energy follow the Kamlet-Taft or Catalán solvent acidity parameter (α or SA) (Figs 8 and 9), while the quality of fit is better for the relaxed excited state (a larger changes in the position of emission spectra) than for the locally excited Franck-Condon state.

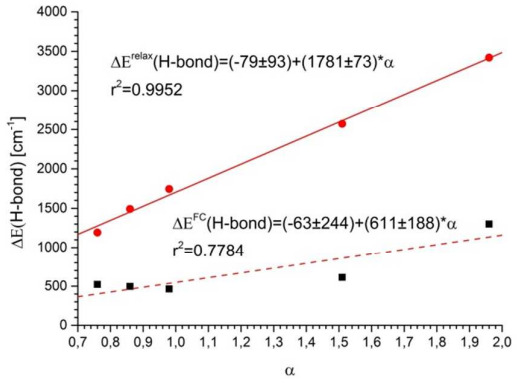

Fig. 8 The hydrogen bond energy changes in locally excited Franck-Condon excited state (dashed line) and relaxed excited state (solid line) as a function of Kamlet-Taft solvent acidity parameter (α).

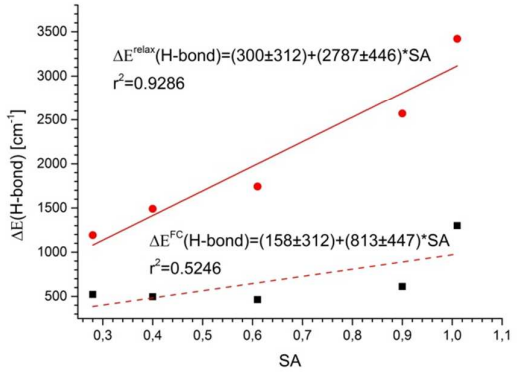

Fig. 9 The hydrogen bond energy changes in locally excited Franck-Condon excited state (dashed line) and relaxed excited state (solid line) as a function of Catalán solvent acidity parameter (SA).

Moreover, the quality of fit is better using Kamlet-Taft solvent acidity parameter (α) than Catalán parameter (SA). 3,6-Di-tert-butyl-8H-indolo[3,2,1-de]acridin-8-one can form two types of hydrogen bonds. One with lone-pair of nitrogen atom and two hydrogen bonds with lone-pairs of oxygen atom. In the excited state intramolecular charge transfer from the amino group to the carbonyl group occurs. This results in a change of the dipole moment as well as the change in the energy of hydrogen bonds. A hydrogen bond formed by a lone pair of nitrogen atom is weakened whereas those formed by a carbonyl group strengthens. After solvent relaxation, the strength of hydrogen bond formed by oxygen atom increases and simultaneously increases the dipole moment in the relaxed excited state. A smaller bathochromic shift of absorption spectra compared to the emission spectra indicates that dipole moment in the excited Franck-Condon state is smaller than in the relaxed excited state.

3.5 Calculations of dipole moment in excited state

According to Bilot-Kawski theory[18-21], the change of dipole moment in the excited state can be calculated, basing on the spectroscopic data, from following equations:

$$\tilde{\nu}_{abs}^{\max} - \tilde{\nu}_{fluo}^{\max} = m_1 f_{BK}(\varepsilon, n^2) + const$$
$$\tilde{\nu}_{abs}^{\max} + \tilde{\nu}_{fluo}^{\max} = -m_2[f_{BK}(\varepsilon, n^2) + 2g(n)] + const \quad (12)$$

where $f(\varepsilon,n^2)$ is given by eq. (9) while

$$g(n) = \frac{3(n^4-1)}{2(n^2+2)^2} \quad (13).$$

Using a slope obtained from eq. (12) and knowing the ground state dipole moment (μ_g), the excited state dipole moment can be calculated using equation,

$$\mu_e = \sqrt{\mu_g^2 + m_2 \beta a^3} \quad (14)$$

where: a is Onsager`s interaction radius of the solute and $\beta=2\pi\varepsilon_0 hc=1.10511044\text{x}10^{-35}$ C^2 is the universal constant. If ground and excited state dipole moments are not parallel, an angle ψ between them can be calculated according to equation (15):

$$\cos\varphi = \frac{1}{2\mu_g\mu_e}[(\mu_g^2+\mu_e^2) - \frac{m_1}{m_2}(\mu_e^2-\mu_g^2)] \quad (15)$$

To calculate the excited state dipole moment, the ground state dipole moment is necessary. It was obtained from theoretical calculation performed applying DFT method with a def2-TZVP basis set (TURBOMOLE v. 6.1) and is equal to μ_g=4.32 D. The calculation of excited state dipole moment value was performed taking into account only saturated hydrocarbons and 1-chloro-n-alkanes. The correlation of spectral properties with Bilot-Kawski solvent polarizability functions according to eq. (12) are satisfactory (r^2=0.9623, m_1=1063 cm^{-1} and r^2=0.9853, m_2=1763 cm^{-1}, respectively) (Figs 14 ESI and 15 ESI). The calculated excited state dipole moment using Onsager`s cavity radius equal to a=6.63 Å is equal to μ_e=8.35 D whereas an angle between the ground and excited state dipole moment is 36^0. Thus, the excited state dipole moment is about two times larger than in the ground state. Apart from the rigid structure of 3,6-di-tert-butyl-8H-indolo[3,2,1-de]acridin-8-one a meaningful change of the angle between ground and excited state dipole moments is observed indicating on the substantial modification of charge distribution in the relaxed excited state. As mentioned above, the excited state dipole moment was calculated taking into account saturated hydrocarbons and 1-chloro-n-alkanes only. In Figs 14 ESI and 15 ESI, the best fit to the equations (12) considering all solvents except alcohols (dashed line) are also shown. The quality of fit is of course worse, however, the slope differs only slightly from the value of slope obtained for saturated and 1-chloro-n-hydrocarbons resulting in a small change of the calculated dipole moment compared to that calculated for saturated and 1-chloro-hydrocarbons solvents. The solvatochromic plot of $\nu_{abs}^{\max}$ and $\nu_{fluo}^{\max}$ *versus* $f_{BK}(\varepsilon,n^2)$ for all studied solvents are shown in Fig. 16 ESI. Omitting the data for alcohols, it should be noted that

the largest deviation from linearity is observed for solvents with a quadrupole moment and with a single bond dipole moment, and for solvents with bond dipole centered at a single atom. These solvents appear more polar locally to optical probe molecule than expected on the basis of bulk dielectric constant [39]. The correlation of the Stokes shift with the microscopic solvent polarity parameter E_T^N can be applied to calculate the dipole moment change between the excited and ground state. According to the equation proposed by Ravi et al.[40] and Kumar at al.[41], the problem associated with the Onsager`s radius estimation can be minimized since a ratio of two Onsager`s radii is involved according to equation (16):

$$\nu_{abs}^{\max} - \nu_{fluo}^{\max} = 11307.6\left[\left(\frac{\Delta\mu}{\Delta\mu_B}\right)^2\left(\frac{a_B}{a}\right)^3\right]E_T^N + const \quad (16)$$

where $\Delta\mu_B$ and a_B are the dipole moment change ($\Delta\mu=\mu_e-\mu_g$) and Onsager's radius, respectively, for a pyridinium N-phenolate betaine dye used to determine the E_T^N values ($\Delta\mu_B$=9 D and a_B=6.2 Å), whereas $\Delta\mu$ and a are the corresponding quantities for the molecule under study. The slope of dependence of Stokes shift *vs*. E_T^N parameter is equal to 2736 (Fig. 3 ESI) which according to equation (16) gives $\Delta\mu$=4.8 D and thereby μ_e=9.1 D. This value is larger than that calculated basing on Bilot-Kawski theory, however, in calculation according to eq (16) all solvents studied were used including alcohols.

Conclusions

The observed solvatochromism of 3,6-di-tert-butyl-8H-indolo[3,2,1-de]acridin-8-one is a result of the increase of the excited state dipole moment. Therefore the solvent-dependent spectroscopic and photophysical properties were analyzed using the Reichard's as well as Kamlet-Taft and Catalán solvent scales. The analysis of these relationships leads to the conclusion that the solvent polarity and solvent hydrogen-bonding donor ability have major influence on measured values. The radiationless deactivation rate constant value decreases with a decrease of the $\Delta E(S_1-S_0)$ energy gap not only for molecule but also for hydrogen-bonded complex. It means that the increase of solvent polarity causes the decrease of S_1-T intersystem rate constant and thereby decreases the intersystem crossing which seems to be the main route of deactivation of the excited state.

Additionally, the spectroscopic properties of this compound were investigated in protic and non-protic solvents and the results were discussed in terms of hydrogen-bonding. It was experimentally found that 3,6-di-tert-butyl-8H-indolo[3,2,1-de]acridin-8-one forms hydrogen bonds which are overall strengthened in the locally excited Franck-Condon and relaxed excited states compared to that of the ground state.

Acknowledgements

This work was financially supported by the grant for Young Scientists No. 538-8443-B046-13 from the University of Gdańsk.

Notes and references

Faculty of Chemistry, University of Gdańsk
Wita Stwosza 63, 80-308 Gdańsk, Poland
* corresponding author, e-mail wieslaw.wiczk@ug.edu.pl

† Electronic Supplementary Information (ESI) available: [includes correlations of spectral and photophysical parameters with Reichardt`s solvent polarity parameter E_T^N, luminescence spectra at 77 K as well as the correlation of the difference and the sum of absorption and emission maxima *versus* Bilot-Kawski polarity functions]. See DOI: 10.1039/b000000x/

1 P. Belmont, J. Bosson, T. Godet, M. Tiano, *Anticancer Agents Med.Chem*., 2007, **7**, 139.
2 G. Cholewiński, K. Dzierzbicka, A. M. Kołodziejczyk, *Pharmacol Rep*., 2011, **63**, 305.
3 A. F. Valdés, *Open Med. Chem.,*2011, **5**, 11.
4 P. Yang, Q. Yang, L. Tong, X. Li, *J. Photochem. Photobiol. B:Biol.,* 2006, 84, 221.
5 Y. Hagivara, T. Hasegawa, A. Shoji, M. Kuwahara, H. Ozaki, H. Sawai, *Bioorg. Med. Chem*., 2008, **16**, 7013.
6 C. Gao, S. Li, X. Lang, H. Liu, F. Liu, C. tan, Y. Jiang, *Tetrahedron*, 2012, **68**, 7920.
7 B. Qiu, L. Guo, Z. Chen, Y. Chi, L. Zhang, G. Chen, *Biosens. Bioelectron*., 2009, **24**, 1281.
8 S. Cosnier, P. Mailley, *Analyst*, 2008, **133**, 984.
9 P. Suppan, N. Ghoneim, Solvatochromism, The Royal Society of Chemistry, Cambridge, U.K., 1997.
10 E. Krystkowiak, K. Dobek, A. Maciejewski, *J. Photochem. Photobiol. A:Chem.,* 2006, **184**, 250.
11 G.-J. Zhao, K.-L. Han, *Acc. Chem. Res*., 2012, **45**, 404.
12 K. Guzow, M. Milewska, W. Wiczk, *Spectrochim. Acta A*, 2005, **61**, 1133.
13 K. Guzow, A. Ceszlak, M. Kozarzewska, W. Wiczk, *Photochem. Photobiol. Sci.,* 2011, **10**, 1610.
14 K. Guzow, M. Czerwińska, A. Ceszlak, M. Kozarzewska, M. Szabelski, C. Czaplewski, A. Łukaszewicz, A. A. Kubicki, W. Wiczk, *Photochem. Photobiol. Sci.,* 2013, **12**, 284.
15 A. Filarowski, M. Kluba, K. Cieślik-Boczula, A. Koll, A. Kochel, L. Pandey, W. M. De Borggrave, M. van der Auweraer, J. Catalán, N. Boens, *Photochem. Photobiol. Sci*., 2011, **9**, 996.
16 C. Reichardt, *Chem. Rev*., 1994, **94**, 2319.
17 C. Reichardt, E. Harbusch-Görnert, *Liebigs Ann. Chem*., 1983, 721.
18 A. Kawski, in: J. F. Rabek (Ed.), Progress in Photochemistry and Photophysics, vol. 5, CRC Press, Boca Raton, USA, 1992, pp. 1–47.
19 A. Kawski, P. Bojarski, in: P. R. Somani (Ed.), Chromic Materials, Phenomena and Their Technological Applications, Applied Science Innovations, 2009, pp. 114-163.
20 L. Bilot, A. Kawski, *Naturforsch.* 1962, **17a**, 621.
21 L. Bilot, A. Kawski, *Naturforsch.* 1963, **18a**, 10 and 256.
22 M. J. Kamlet, J.-L. M. Abbound, R. W. Taft, *Prog. Phys. Org. Chem*., 1982, **13**, 485.
23 J. Catalán, *J. Phys. Chem. B*, **113** (2009) 5951.
24 W. Zhao, L. Pang, W. Bian, J. Wang, *ChemPhysChem*, 2008, **9**, 1593.
25 E. Krystkowiak, K. Dobek, A. Maciejewski, *Photochem. Photobiol. Sci*., 2013, **12**, 446.
16 E. Krystkowiak, K. Dobek, G. Burdziński, A. Maciejewski, *Photochem. Photobiol. Sci*., 2012, **11**, 1322.
27 E. Krystkowiak, A. Maciejewski, *Phys. Chem. Chem. Phys*., 2011, **13**, 11317.
28 F. C. Chipen, A. Mishra, G. Krishnamoorthy, *Phys. Chem. Chem. Phys*., 2012, **14**, 8775.
29 Y. Liu, M. Nishiura, Y. Wang, Z. Hou, *J. Am. Chem. Soc*., 2006, **128**, 5592.

30 M. V. Skorobogatyi, A. A. Pchelintseva, A. L. Petrunina, I. A. Stepanova, V. L. Andronova, G. A. Galegov, A. D. Malakhov, V. A. Korshun, *Tetrahedron*, 2006, **62**, 1279.
31 J. R. Lakowicz, Principles of Fluorescence Spectroscopy, 2nd ed., Kluwer Academic/Plenum Publishers, New York, 1999.
32 M. Baruah, W. Qin, C. Flores, J. Hofkens, R. A. L. Valle, D. Beljonne, M. Van der Auweraer, W. M. De Borggrave, N. Boens, *J. Phys. Chem. A,* 2006, **110**, 5998.
33 J. Jayabarathi, V. Thanikachalam, K. Jayamoorthy, *Photochem. Photobiol. Sci*., 2013, **121,** 761.
34 R. Englman, J. Jortner, M*ol. Phys.,*1970, **18**, 145.
35 Postgraduate Chemistry Series. Photochemistry of Organic Compounds. From Concept to Practice, P. Klán, J. Wirz, J. Wiley & Sons Lt., 2009, UK
36 N. J. Turro, V. Ramamuthry, J. C. Scaiano, Principles of Molecular Photochemistry. An Introduction, Chapter 5, University Science Book, Sausalito, California, 2009.
37 R. Lopez-Artega, A. B. Stephansen, C.A. Guarin, T.I. Solling, J. Peon, *J. Phys. Chem. B,* 2013, **117**, 9947.
38 X. Liu, J.M. Cole, K.S. Low, *J. Phys. Chem. C*, 2013, **117**, 14731.
39 I. Renge, *J. Phys. Chem. A*, 2010, **114**, 6250.
40 M. Ravi, A. Samanta, T. P. Radharkrishnan *J. Phys. Chem. A*, 1994, **98**, 9133.
41 S. Kumar, V.C. Rao, R. C. Rostogi, *Spectrochim. Acta*, *Part A*, 2001, **57**, 41.

Journal Name RSCPublishing

ARTICLE

Table 1. Spectroscopic and photophysical properties of 3,6-di-tert-butyl-8H-indolo[3,2,1-de]acridin-8-one in solvents used.

nr	Solvent	ν_{abs} [cm^{-1}]	ν_{em} [cm-1]	$\Delta\nu$ [cm^{-1}]	φ	τ [ns]	k_f*10^{-7} [s^{-1}]	$k_{nr}*10^{-7}$ [s^{-1}]
1	MeOH	24038	21598	2440	0.469	5.71	8.28	9.30
2	EtOH	24038	21882	2156	0.445	5.20	8.56	10.67
3	iPrOH	23981	22222	1759	0.396	4.59	8.64	13.15
4	TFE	23889	20790	3019	0.532	6.09	8.73	7.69
5	HFiP	23202	20000	3202	0.689	6.69	10.30	4.65
6	Hexane	24752	24450	302	0.010	0.98	0.98	101.06
7	Isooctane	24752	24331	421	0.010	0.98	1.04	101.00
8	Hexadecane	24630	24253	277	0.034	0.85	4.02	113.62
9	Squalene	24610	24301	309	0.047	0.82	5.79	116.16
10	Cyclohexane	24691	24331	360	0.010	0.91	1.11	108.78
11	Toluen	24331	23640	691	0.251	1.12	22.42	66.87
12	1-chloropropane	24501	23584	926	0.164	1.47	11.14	56.89
13	1-chlorobutane	24510	23584	926	0.127	1.37	9.29	63.70
1`4	1-chlorohexane	24510	23697	813	0.112	1.11	10.09	80.00
15	1-chlorooctane	24510	23753	757	0.103	1.07	9.59	83.87
16	1-chlorodecane	24510	23780	730	0.056	0.96	5.85	98.31
17	1-chlorohexadecane	24510	23864	646	0.034	0.78	4.38	123.82
18	Acetone	24390	23148	1242	0.226	2.28	9.92	33.94
19	Acetonitrile	24331	22831	1500	0.253	3.21	7.87	23.29
20	Dioxane	24450	23364	1086	0.229	1.52	15.06	50.73
21	THF	24450	23640	810	0.149	1.35	11.04	63.03
22	MeTHF	24510	23471	1039	0.134	1.17	11.48	73.99
23	Et_2O	24630	23302	1328	0.272	0.36 (α=0.46) 1.44 (α=0.54)	--	--
24	AcOEt	24510	23584	926	0.134	1.41	9.48	61.44
25	DMF	24272	22831	1441	0.325	2.91	11.18	23.18
26	DMSO	24096	23256	840	0.388	3.38	11.49	18.10

Table 2 Estimated coefficients (y_0, a_{SP}, b_{SdP}, c_{SB}, d_{SA}), their errors and correlation coefficients (r^2) for multi-linear correlation analysis of ν_{abs}, ν_{fluo}, φ, τ, Δν, k_f, k_{nr} of compound as a function of the Catalán four-parameter solvent scale (eq. 7).

	y_0	a_{SP}	b_{SdP}	c_{SB}	d_{SA}	r^2	N
ν_{abs} [cm^{-1}]	25601±257	-(1355±376)	-(229±84)	-(172±109)	-(873±119)	0.9190	20
ν_{fluo}	23836±743	608±1087	-(973±243)	-(450±316)	-(2711±343)	0.9510	20
[cm^{-1}]	24248±101	-	-(945±232)	-(451±309)	-(2711±343)	0.9500	
Δν [cm^{-1}]	1774±668	-(2007±978)	752±218	318±284	1777±308	0.9311	20
φ	-(0.347±0.186)	0.566±0.273	0.122±0.061	0.163±0.079	0.497±0.086	0.8879	20
$\tau*10^9$	0.626±1.160	0.113±2.378	1.105±0.508	1.404±0.686	5.280±0.719	0.9368	19
[ns]	0.702±0.205	-	1.108±0.487	1.407±0.659	5.258±0.534	0.9368	
k_f*10^{-8}	-(3.020±1.382)	5.262±2.010	0.488±0.429	-(0.158±0.580)	0.616±0.607	0.4552	19
[s^{-1}]	-(2.130±0.986)	3.945±1.412	0.581±0.243	-	-	0.4389	
$k_{nr}*10^{-9}$ [s^{-1}]	1.345±0.447	-(0.426±0.652)	-(0.630±0.139)	-(0.286±0.188)	-(0.511±0.197)	0.9017	19
	1.056±0.057	-	-(0.641±0.136)	-(0.299±0.183)	-(0.429±0.149)	0.8987	

Table 3 Estimated coefficients (y_0, a_{π^*}, b_α, c_β), their errors and correlation coefficients (r^2) for multi-linear correlation analysis of ν_{abs}, ν_{fluo}, φ, τ, $\Delta\nu$, k_f, k_{nr} of compound as a function of the Kamlet-Taft solvent scale (eq. 6).

	y_0	a_π^*	b_α	c_β	r^2	N
ν_{abs} [cm^{-1}]	24720±50	-(491±119)	-(492±48)	-(20±107)	0.9231	20
	24718±50	-(505±90)	-(489±45)	-	0.9139	
ν_{fluo}[cm^{-1}]	22224±94	-(1122±227)	-(1758±92)	-(306±203)	0.9731	20
	24205±97	-(1334±184)	-(1719±97)	-	0.9693	
$\Delta\nu$ [cm^{-1}]	478±113	630±272	1258±110	231±244	0.9241	20
	497±115	852±218	1216±108	-	0.9160	
φ	0.027±0.02)	0.248±0.058	0.238±0.023	0.097±0.052	0.9306	20
$\tau*10^9$ [ns]	0.764±0.188	0.944±0.454	2.917±0.177	1.683±0.403	0.9638	19
k_f*10^{-7}[s^{-1}]	3.509±1.850	15.023±4.463	-(1.812±1.735)	-(4.370±3.965)	0.4704	19
	3.321±1.834	11.103±3.251	-	-	0.4070	
$k_{nr}*10^{-8}$ [s^{-1}]	10.444±0.444	-(6.786±1.073)	-(3.110±0.417)	-(3.627±0.953)	0.9441	19

Table 4. Hydrogen bond energy changes after photoexcitation of 3,6-di-tert-butyl-8H-indolo[3,2,1-de]acridin-8-one in alcohols calculated based on solvatochromic plot of absorption and emission spectra.

solvent	ΔE(H-bond) [cm^{-1}]		Kamlet-Taft (α) and Catalan (SA) solvent H-bond donating parameter	
	S_1^{FC}	S_1^{relax}	α	SA
iPrOH	522	1193	0.76	0.28
EtOH	496	1491	0.86	0.40
MeOH	463	1744	0.98	0.61
TFE	612	2570	1.51	0.90
HFIP	1300	3421	1.96	1.01

Journal Name

RSCPublishing

ARTICLE

Solvatochromic properties of 3,6-di-tert-butyl-8H-indolo[3,2,1-de]acridin-8-one

Cite this: DOI: 10.1039/xoxxoooooox

Received ooth January 2012,
Accepted ooth January 2012

DOI: 10.1039/xoxxoooooox

www.rsc.org/

Marlena Czerwińska, Małgorzata Wierzbicka, Katarzyna Guzow, Irena Bylińska, Wiesław Wiczk*

Abstract

The spectral and photophysical properties of newly synthesized 3,6-di-tert-butyl-8H-indolo[3,2,1-de]acridin-8-one were studied. To determine the contribution of specific and nonspecific interactions of this compound with solvents, the solvatochromic methods were used. It was found that bathochromic shifts of absorption and fluorescence spectra were mostly caused by polarizability/dipolarity interactions of the solute with solvent. The excited state dipole moment, determined based on solvatochromic method, is two times higher than that in the ground state. Also, the spectral and photophysical properties of compound studied correlate with E_T^N solvent polarity scale. The radiative rate constant does not depend on the solvent properties, while the non-radiative rate constant decreases with increasing solvent polarity. Such decrease of non-radiative rate constant with lowering of energy gap between S_0 and S_1 states indicates on the participation of triplet state in the deactivation of the excited state. After photoexcitation hydrogen bond energy increases in both locally excited Franck-Condon and relaxed excited state, however, the change of hydrogen bonds energy is three times higher in the relaxed excited state. The hydrogen bond energy change measured in five alcohols correlates with the Kamlet-Taft or Catalán solvent acidity parameter.

Journal Name RSCPublishing

ARTICLE

1 Introduction

It is well known that natural and synthetic acridines/acridones possesses antitumor activity[1-3] and DNA photo-damaging ability[4]. Their biological activity is mainly attributed to the planarity of these aromatic compounds, which enables intercalation within the double-stranded DNA structure, thus interfering with the cellular machinery. Besides biological activity, acridone and its derivatives exhibit a high fluorescence quantum yield and characterized by a high photostability. For this reason, are used, among others, as a sensor for fluorescence detection of DNA[5-8]. Studied compound 3,6-di-tert-butyl-8H-indolo[3,2,1-de]acridin-8-one belongs to the acridone group comprising many potential drugs or fluorescent probe. To determine whether it is suitable as a fluorescent sensor the factors influencing photophysical properties should be determined. To establish what type of interactions are important ones in the solute-solvent interactions, we performed a detailed study of the environmental impact on spectral and photophysical properties of 3,6-di-tert-butyl-8H-indolo[3,2,1-de]acridin-8-one.

It is commonly acknowledged that solvent-dependent UV–Vis spectral band shifts can arise from either general and/or specific solvent effects[9]. The first effect results from isotropic interactions of the chromophore dipole moment with the reaction field induced in the surrounding solvent. Specific effects result from the short-range anisotropic interactions between the chromophore with one or more solvent molecules in its first solvation shell, an important example of which is the formation of hydrogen bonds. It is thus of interest to quantify the relative contributions from these two effects[10,11]. The electronic transition in molecules, involving intramolecular charge transfer, is very sensitive to the nature of the microenvironment around the solute and the spectral parameters can be used to study solute-solvent interactions at the microscopic level[12-15]. In the case of different electron densities in the electronic ground and excited state of a light-absorbing molecule, its dipole moment varies in these two states. Thus, a change of the solvent affects the ground and excited state differently. The solvent-dependent photophysical characteristic can be investigated by steady-state absorption and emission spectroscopy as well as time-resolved fluorimetry. From these experiments, the position of the spectra maxima, the Stokes shift, fluorescence lifetime and the rate constants of radiative and non-radiative deactivation of compound studied are determined[12-15]. The normalized E_T^N polarity scale[16,17], Bilot-Kawski solvent polarizability functions[18-21], and Kamlet-Taft[22] and Catalán[23] multi-parameters solvent scales are used to describe the solvent effect on the spectral and photophysical properties. The changes of the hydrogen bond after excitation are also addressed[10,24-28]. In this work, applying the solvatochromic methods the influence of solvents on the spectral and photophysical properties and hydrogen bond energy changes after photoexcitation as well as multi-linear correlations of newly synthesized 3,6-di-tert-butyl-8H-indolo[3,2,1-de]acridin-8-one (**3**, Fig. 1), are presented.

2 Experimental

2.1 Synthesis

Synthesis of 3,6-di-tert-butyl-8H-indolo[3,2,1-de]acridin-8-one was performed according to the scheme (Fig. 1).

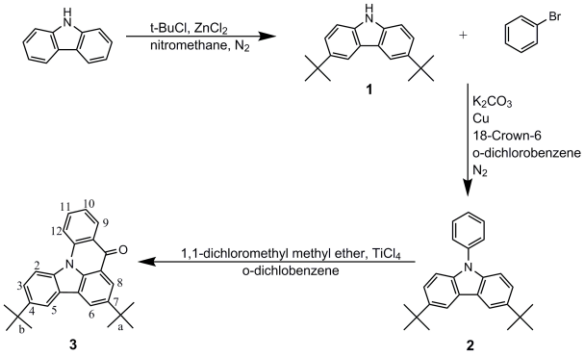

Fig. 1 Scheme of 3,6-di-tert-butyl-8H-indolo[3,2,1-de]acridin-8-one synthesis.

To obtain 3,6-di-tert-butyl-9*H*-carbazole (compound 1) and 9-phenyl-3,6-di-tert-butyl-9*H*-carbazole (compound 2) literature procedures were applied[29]. Both compounds were purified by column chromatography (Merck, Silica gel 60, 0.040-0.063 mm, eluent: CH_2Cl_2:petroleum ether 1:10 (v/v) (compound 1), CH_2Cl_2:petroleum ether 1:5 (v/v) (compound 2)) and then crystallized from boiling petroleum ether. Compound 1 was obtained with 46% yield whereas compound 2 with 29% yield. The title compound **3** was obtained applying procedure described in[30]. To a stirred solution of 9-phenyl-3,6-di-tert-butyl-9*H*-carbazole (compound **2**) (0.09 g, 0.253 mmol) in 1,2-dichlorobenzene (5 ml) cooled in an ice bath, 1,1-dichloromethyl methyl ether (0.033 ml, 0.365 mmol) and $TiCl_4$ (0.046 ml, 0.419 mmol) were added. The reaction was continued for 1 hour in the ice bath. Then the reaction mixture was allowed to warm up to the room temperature and poured on ice (14.05 g) and concentrated HCl (0.63 ml). The organic layer was diluted with chloroform, washed with a 5% solution of HCl (1x) and water (3x) and dried with anhydrous Na_2SO_4. After evaporation the residue (yellow solid) was purified by column chromatography (Merck, Silica gel 60, 0.040–0.063 mm) using a mixture of CH_2Cl_2:petroleum ether 1:2 (v/v) as an eluent. Additional purification was performed using RP-HPLC (Kromasil column, C-8, 5 μm, 250 mm long, i.d.=20 mm; linear gradient 50-100%B over 120 minutes, A=0.1% water solution of trifluoroacetic acid, B=80% of acetonitrile in A) giving desired compound as a yellowish-orange solid (0.064 g, 0.168 mmol, 66% yield). The purity of the obtained compound was checked by RP-HPLC using analytical column Phenomenex Jupiter® (C-18, 5 μm, 250 mm long, i.d.=4.6 mm, gradient 50-100% B over 30 minutes, λ=223 nm, 245 nm, 300 nm, t_R=28.3 min.). The product was identified by means of the ^1H and ^1H-^1H COSY NMR (Bruker AVANCE III spectrometer (500 MHz) in $CDCl_3$), IR spectrum (Bruker IFS-66 instrument) and mass spectrum (Bruker Biflex III (MALDI-TOF)). m.p. 237-241 °C; MS: m/z=382.2 $(M+H)^+$; IR (KBr): ν_{max} (cm^{-1}) 2867.7-2953.9 CH; 1648.0 C=O; 1442.6-1484.0 C=C; 1144.6-1264.4 $C(CH_3)_3$; ^1H NMR: δ (ppm) 1.537 (s, 9H, $(CH_3)_3$ (a)); 1.581 (s, 9H, $(CH_3)_3$ (b)); 7.497-7.529 (m, 1H, $C^{11}H$); 7.714 (dd, 1H, C^3H, J=2.0 Hz, J=8.8 Hz); 7.920-7.955 (m, 1H, $C^{10}H$); 8.247-8.264 (m, 2H, C^2H, C^8H); 8.495 (d, 1H, C^9H, J=8.5 Hz); 8.532 (d, 1H, C^5H, J=2.0 Hz), 8.551 (d, 1H, C^6H, J=2.0 Hz); 8.757 (dd, 1H, $C^{12}H$, J=1.5 Hz, J=8.0 Hz). In 2D NMR ^1H-^1H COSY spectrum the following correlation signals were observed: the coupling of $C^{11}H$ (δ=7.5 ppm) with $C^{10}H$ (δ=7.9 ppm) and $C^{12}H$ (δ=8.8 ppm), the coupling of $C^{10}H$ (δ=7.9 ppm) with

C^9H (δ=8.5 ppm), the coupling of C^3H (δ=7.7 ppm) with C^2H (δ=8.2 ppm). For hydrogen atoms C^5H, C^6H and C^8H no correlation signals were observed indicating on the absence of their coupling with other hydrogen atoms present in the molecule.

2.2 Spectroscopic measurements

The UV/Vis absorption spectra in all 26 solvents studied were measured using a Perkin-Elmer Lambda 40P spectrophotometer, whereas emission spectra were measured using a Horiba-Jobin Yvon FluoroMax-4 spectrofluorimeter. Solvents of the highest available quality were used. Fluorescence quantum yields (Φ) were calculated with quinine sulphate in 0.5 M H_2SO_4 (Φ= 0.53 ± 0.02) as reference and were corrected for different refractive indices of solvents[31]. In all fluorimetric measurements, the optical density of the solution does not exceed 0.1. Luminescence spectra were measured in quartz capillaries at liquid nitrogen temperature using a low-temperature accessory. The fluorescence lifetimes were measured with a time-correlated single-photon counting apparatus Edinburgh CD-900 equipped with NanoLed N16 (UV LED λ=339 nm) from IBH as the excitation source. The half-width of the response function of the apparatus, measured using a Ludox solution as a scatter, was about 1.0 ns. The emission wavelengths were isolated using a monochromator. Fluorescence decay data were fitted by the iterative convolution to the sum of exponents according to eq.:

$$I(t) = \sum_i \alpha_i \exp(-t/\tau_i) \quad (1)$$

where α_i is the pre-exponential factor obtained from the fluorescence intensity decay analysis and τ_i the decay time of the i-th component, using a software supported by the manufacturer. The adequacy of the exponential decay fitting was judged by visual inspection of the plots of weighted residuals as well as by the statistical parameter χ^2_R and shape of the autocorrelation function of the weighted residuals and serial variance ratio (SVR).
Linear and multi-parametric correlations were performed using Origin v. 9 software.

3 Results and discussion

3.1 Spectral properties

Absorption spectra of the title compound in selected solvents are presented in Fig. 2, whereas the emission spectra in Fig. 3.

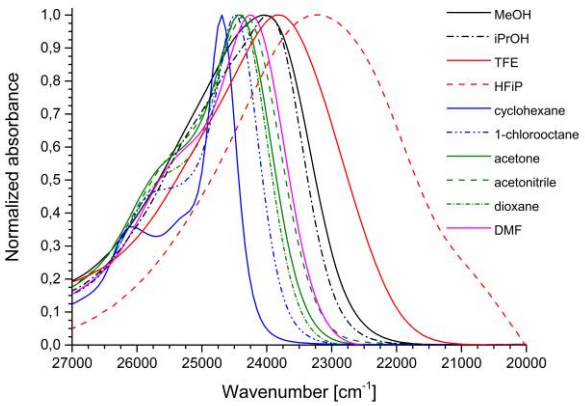

Fig. 2 Absorption spectra of 3,6-di-tert-butyl-8H-indolo[3,2,1-de]acridin-8-one in selected solvents.

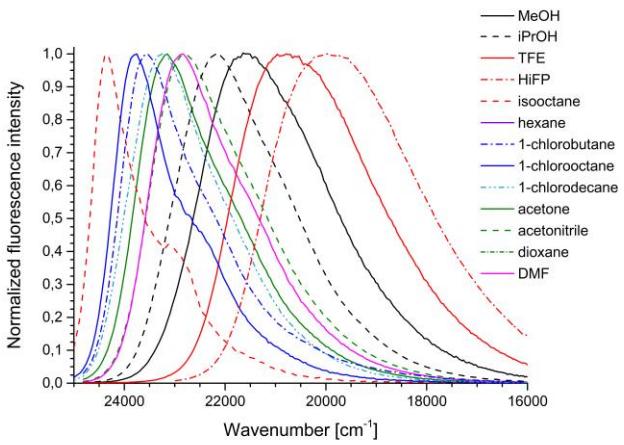

Fig. 3 Emission spectra of 3,6-di-tert-butyl-8H-indolo[3,2,1-de]acridin-8-one in selected solvents.

In non-polar solvents, saturated hydrocarbons and 1-chloroalkanes, absorption spectrum possesses a maximum at about 24700 cm^{-1}. The spectra in these solvents have small half-width and the most intense is the first vibronic band with poorly separated vibrational structure on the short-wavelength side of the spectrum. The increase of solvent polarity causes bathochromic shift of the spectrum and the simultaneous loss of the vibrational structure. In protic solvent, the long-wavelength absorption band takes bell shape form and the position of its maximum shifts with increasing proton-donor capacity of the solvent. However, the bathochromic shift of the absorption band is not substantial and ranges from 24690 cm^{-1} for cyclohexane to 24100 cm^{-1} in MeOH. A larger bathochromic shift is observed for TFE (2,2,2-trifluoroethanol) (23700 cm^{-1}) and HFIP (1,1,1,3,3,3-hexafluoro-2-propanol) (22990 cm^{-1}).

More substantial changes are observed in emission spectra (Fig. 3). In non-polar solvents the emission spectra possess a maximum at about 24100 cm^{-1} with weakly marked vibrational structure. An increase of solvent polarity results in bathochromic shift of the spectrum and loss of its vibrational structure. Like for absorption spectra, a major bathochromic shift of emission band is observed in alcohols. The larger proton-donor properties of alcohol, the greater shift is observed (position of the emission band maximum is located at 22200 cm^{-1} for 2–propanol whereas at 19800 $cm^{-1}$for HFIP). The spectral and photophysical properties of compound studied are gathered in Table 1.

Solvent properties influences fluorescence quantum yield and fluorescence lifetime of the studied compound (Table 1). Larger fluorescence quantum yields are observed in alcohols (up to 0.69 for HFIP) and polar solvents whereas for non-polar solvents these values are relatively small (about 0.01 for hexane). Similarly, fluorescence lifetimes are longer for protic and polar solvents (about 6.7 ns for HFIP) and much shorter for non-polar solvents (0.98 ns for hexane). It should be noted that in all solvents studied the fluorescence intensity decay is mono-exponential, except ethyl ether in which fluorescence intensity decay of 3,6-di-tert-butyl-8H-indolo[3,2,1-de]acridin-8-one is bi-exponential indicating on its specific interaction with this solvent.

3.2 Correlation with Reichardt's E_T^N solvent polarity scale parameter

The various models of solvation, several empirical solvent polarity parameters have been proposed to characterize and rank empirically the polarity of a solvent[16,17,22,23]. One of the most popular solvent polarity scale is the $E_T(30)$ scale, based on Vis spectroscopic band shifts of a negatively solvatochromic

standard probe[16,17], or the normalized E_T^N parameter defined according to equation (2):

$$E_T^N = \frac{E_T(solvent) - E_T(TMS)}{E_T(water) - E_T(TMS)} \quad (2)$$

where TMS denotes tetramethylsilane. They are mostly used to correlate the absorption or emission transition energies and Stokes shifts[13-15,32,33].

As mentioned above, the maxima of absorption spectra shift to the red with increasing solvent polarity. The plot of dependence of wavenumber of maximum of absorption spectrum *versus* E_T^N (Fig. 1 ESI) reveals rather week correlation (r^2=0.8812, N=21). Main reason for the lack of good correlation is large deviations observed for alcohols, especially for TFE and HFIP, but also for other solvents such as toluene or DMSO. This indicates on a specific solute-solvent interactions. Separate analyses of the data for the protic and non-protic solvents do not improve the correlation. For non-protic solvents correlation coefficient is r^2=0.7349 for 16 solvents whereas for protic ones r^2=0.6745 (N=5) (Fig. 1 ESI). A better correlation with Reichardt`s solvent polarity parameter (E_T^N) (r^2=0.9554, N=21) was obtained for the position of emission maximum (Fig. 2 ESI). However, the experimental points for non-protic solvents are grouped in three clusters of points which give bad correlation coefficient (r^2=0.7645, N=16) with E_T^N, in opposite to protic solvents (r^2=0.9823, N=5). The Stokes shift correlates well with the E_T^N parameter after the rejection of the points corresponding to ethyl ether and DMSO, (r^2=0.9829, N=19) and there is no reason to analyse separately protic and non-protic solvents (Fig. 3 ESI). Also, the dependence of fluorescence quantum yield on E_T^N parameter does not give rise to a division of solvents into two groups, however, the correlation coefficient is rather small (r^2=0.8848, N=21) due to the large deviation from a straight line observed for polar solvents (Fig. 4 ESI). The dependence of fluorescence lifetime can be described as a straight-line dependence on E_T^N parameter with good correlation coefficient (r^2=0.9594, N=20, Fig. 5 ESI). However, it can be seen that the fluorescence decay time values measured in alcohols clearly differ in a systematic way from this relationship. A separate analysis of fluorescence lifetime dependence on E_T^N for protic and non-protic solvents (Fig. 5 ESI) gave a worse value of correlation coefficient for non-protic solvents (r^2=0.8858, N=15), however, a better correlation for protic solvents (r^2=0.9817, N=5).

Both fluorescence quantum yield and fluorescence lifetime are complex function of fluorescence and non-radiative rate constant. For the mono-exponential fluorescence intensity decay, the radiative (k_f) and non-radiative (k_{nr}) rate constants can be calculated from the measured fluorescence quantum yield (Φ) and fluorescence lifetime (τ) according to equations (3) and (4):

$$k_f = \Phi / \tau \quad (3)$$

$$k_{nr} = (1-\Phi) / \tau \quad (4)$$

Therefore, an analysis of these rate constants as a function of E_T^N was performed to receive information which of them and how depend on the solvent parameters, enabling to estimate which path of the excited state deactivation predominates.

It was found that the radiative rate constant (k_f) poorly depends on E_T^N (r^2=0.2319, N=15) (Fig. 6 ESI) even after exclusion of the data corresponding to hydrocarbon solvents. Very large deviation from correlation line of k_f values in hydrocarbon solvents may indicate that in these solvents the fluorescence occurs from a different state than in the other ones.

In the case of dependence of non-radiative rate constant (k_{nr}) on E_T^N parameter, separate analyses for the protic and non-protic solvents have to be performed (Fig. 7 ESI). In both cases, the increase of solvent polarity causes a decrease of non-radiative rate constant as indicated by negative slope –(3.63±0.27), (r^2=0.9334, N=15) for non-protic solvents and -(1.89±0.19), (r^2=0.9695, N=5) for protic ones. Thus, the solute-solvent interactions with polar environment decrease the non-radiative rate constant of 3,6-di-tert-butyl-8H-indolo[3,2,1-de]acridin-8-one. Moreover, this process is slower in alcohols than in non-protic solvents. The strong increase of k_{nr} upon solvent polarity can be rationalized if k_{nr} can be attributed mainly to internal conversion (the energy gap lowering)[15,29]. In the opposite case, the main path of the excited state deactivation is intersystem crossing to the triplet state[30].

According to Englman and Jortner[34] the weak coupling limit (the relative horizontal displacement of the two potential energy surfaces is small) reveals an exponential dependence of the transition probability on the energy gap ΔE. The dependence of non-radiative rate constant on the energy gap between two electronic states can be roughly estimated from equation[35]:

$$\log(k_{IC}) \approx 12 - 2\nu_{fluo}^{max} \quad (5)$$

where: k_{IC} is the rate constant of internal conversion expressed in s^{-1} and ν_{fluo}^{max} expressed in μm^{-1}. As can be seen from the formula (5) the bathochromic shift of fluorescence spectrum causes the increase of the non-radiative rate constant. In the case studied, a bathochromic shift of emission spectra is observed with increase of solvent polarity, however, the decrease of the non-radiative rate constant is recorded. An inverse relationship between non-radiative rate constant (k_{nr}) and the environment polarity and thereby decreasing the energy gap between relaxed excited state and ground state (Fig. 4) is in opposition to that founded in literature[15,29]. The plot of ln(k_{nr}) as a function of energy gap between S_1 and S_0 states ($\Delta E(S_1\text{-}S_0) = \nu_{fluo}^{max}$) gives two straight lines (Fig. 4).

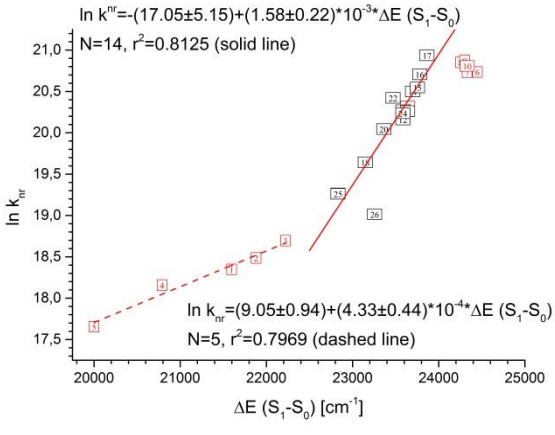

Fig. 4 Correlations between the logarithm of the non-radiative rate constant ln(k_{nr}) and $\Delta E(S_1\text{-}S_0) = \nu_{fluo}^{max}$ energy gap for 3,6-di-tert-butyl-8H-indolo[3,2,1-de]acridin-8-one in studied solvents.

A slope is equal to (1.58±0.22)*10^{-3}, (r^2=0.8125, N=15, without hydrocarbon solvents which form a separate cluster of points) for non-protic solvents and (4.33±0.44)*10^{-4}, (r^2=0.7969, N=5) for protic ones.

To further investigate the dependence of non-radiative rate constant on solvent polarity, luminescence spectra of studied compound were measured in several solvents. In non-polar methylcyclohexane (MeCx), apart from weak fluorescence

spectrum shifted to the red compared to the spectrum measured at room temperature, a strong phosphorescence spectrum is observed (Fig. 8 ESI). This indicates that the main deactivation route of the excited state is the intersystem crossing to the triplet state, hence, low fluorescence quantum yield and short fluorescence lifetime observed in saturated hydrocarbon solvents. The situation is different in protic solvents. In methanol glass only weak phosphorescence is visible as a shoulder on the red-side of the fluorescence spectrum (Fig. 9 ESI). In a weakly polar and polar solvents (MeTHF, C_3H_7Cl, DMF) well separated fluorescence and phosphorescence spectra are observed (Fig. 5, Fig. 10 ESI).

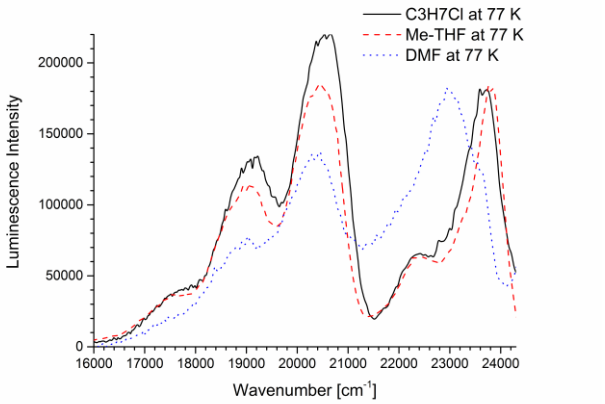

Fig. 5 The luminescence spectra of 3,6-di-tert-butyl-8H-indolo[3,2,1-de]acridin-8-one (normalized to the same fluorescence intensity) in C_3H_7Cl, MeTHF and DMF measured at 77 K.

It is worth mentioning that the phosphorescence spectrum with maximum at 20400 cm^{-1} and well-resolved vibrational structure practically does not depend on solvent polarity, contrary to the fluorescence spectrum. Additionally, the ratio of phosphorescence to fluorescence intensity decreases with an increase of solvent polarity (Fig. 5). To explain such a relationship the interdependence of the internal conversion and intersystem crossing rate constants should be examined. Radiationless rate constant (k_{nr}) is the sum of internal conversion (k_{IC}) and intersystem crossing (k_{ISC}) rate constants. The observed decrease of k_{nr} with decrease of (S_1-S_0) energy gap can be rationalized assuming decrease of intersystem rate constant. One can assume that the excited state lies over two (n,π^*) and ($\pi\pi^*$) states. Two scenarios are possible. In the first one, a decrease of the energy gap between S_1 and S_0 states at the same time lowers the energy of $S_1(\pi\pi^*)$ state below the $T(n,\pi^*)$ state so that it is located between triplet states. According to El-Sayed rule[36], the rate constant of intersystem crossing (k_{ISC}) is greater for $S_1(\pi\pi^*)\rightarrow T(n,\pi^*)$ than for $S_1(\pi\pi^*)\rightarrow T(\pi\pi^*)$ transition. Thus, as a result of the decrease of the energy of excited singlet, the intersystem crossing between $S_1(\pi\pi^*)\rightarrow T(\pi\pi^*)$ state takes place resulting in the decrease of intersystem rate constant and therefore an increase in the fluorescence intensity and decrease in the phosphorescence intensity is observed. Based on such a mechanism the differences in the photophysics of 2-nitrofluorene with that of 2-diethylamino-7-nitrofluorene was explained[37]. A second possible mechanism may result from the reduction of Franck-Condon factor in the $S_1\rightarrow T_1$ intersystem crossing process which is the result of the increase of the ICT participation in the S_1 state (Fig. 11 ESI). In both of these explanation one assumes no effect or little effect of the solvent polarity on the internal conversion rate constant. Based on collected data, the second mechanism seems to be more probable.

Thus, it seems that efficient intersystem crossing to a triplet state determines photophysical properties of 3,6-di-tert-butyl-8H-indolo[3,2,1-de]acridin-8-one (low fluorescence quantum yield and short fluorescence lifetime) in non-polar and weakly polar solvents.

3.3 Multi-parametric correlations

The multiple linear regression, approach of Kamlet and coworkers[22] and Catalán[23], has been used to correlate UV–Vis absorption and emission energies[14,15,38] as well as another photophysical properties with an index of the solvent dipolarity/polarizability which is a measure of the solvent's ability to stabilize a charge or dipole through nonspecific dielectric interactions (π^* or SP and solvent dipolarity SdP in a new generalized solvent polarity Catalán scale), and indices of the solvent's hydrogen-bond donor strength (α or SA) and hydrogen-bond acceptor strength (β or SB) according to eqs: (6) and (7):

$$y = y_0 + a_{\pi^*}\cdot\pi + b_{\alpha}\cdot\alpha + c_{\beta}\cdot\beta \qquad (6)$$

or

$$y = y_0 + a_{SP}\cdot SP + b_{SdP}\cdot SdP + c_{SA}\cdot SA + d_{SB}\cdot SB \quad (7)$$

where: y denotes a solvent-dependent physicochemical property in a given solvent and y_0 the statistical quantity corresponding to the value of the property in the gas phase; π^*, α, β, SP, SdP, SA, SB represent independent solvent parameters accounting for various types of solute–solvent interactions; a_{π^*}, b_{α}, c_{β} and a_{SP}, b_{SdP}, c_{SA} and d_{SB} are adjustable coefficients that reflect the sensitivity of physical property y in a given solvent to the various solvent parameters.

The results of multi-linear correlation according to Catalán and Kamlet-Taft equations are presented in Tables 2 and 3. Both solvent polarity scales predict a bathochromic shift of absorption spectra with increase of solvent polarity (all coefficients in Eqs (6) and (7) are negative). A fair fit was obtained in both cases (r^2=0.9190 for Catalán and r^2=0.9231 for Kamlet-Taft correlation, respectively). In the Catalán equation all four coefficients are important. However, the large values of a_{SP} (51.5%) and d_{SA} (33%) coefficients compared to the others indicate that the changes of ν_{abs} may reflect primarily a change in polarizability and acidity of the environment of the chromophore, whereas the solvent dipolarity (9%) and basicity (6.5%) have a minor influence. The same conclusion can be drown from Kamlet-Taft correlation. Two parameters, solvent dipolarity/polarizability (π^*) and solvent acidity (α), influenced equally (in about 50%) the bathochromic shift of absorption spectra, while solvent basicity can be omitted because of low value and large error exceeding the value of the parameter (the quality of fit decrease a little to r^2=0.9139 comparing to the original fir r^2=0.9231). Good quality of fits were obtained in multi-linear correlations of the position of fluorescence maximum (r^2=0.9510 for Catalán and r^2=0.9731 for Kamlet-Taft correlation). In both cases, solvent basicity has minor influence on bathochromic shift of fluorescence spectrum ($c_{SB}\approx$ 12%), whereas the solvent acidity ($d_{SA}\approx$74%) and solvent dipolarity ($b_{SdP}\approx$26%) have major influence on it. Solvent polarizability in the Catalán equation may be disregarded because of its large error without substantial decrease of the quality of fit (r^2=0.9500 compared to the original fit r^2=0.9510). A similar results were obtained from Kamlet-Taft correlation (r^2=0.9731). A bathochromic shift of fluorescence spectrum is caused mainly by solvent dipolarity/polarizability (35%) and solvent acidity (55%), while solvent basicity has a minor influence (10%). It is worth mentioning that the correlation parameters for both absorption and emission spectra are negative meaning that their changes cause red-shift of the spectra. Additionally, correlation parameters obtained for fluorescence spectra are larger, taking into account their absolute values, than those calculated for absorption spectra. This indicates that the electronic structure of the locally excited Franck-Condon and relaxed excited states of 3,6-di-tert-butyl-

8H-indolo[3,2,1-de]acridin-8-one differ significantly, and the relaxed excited state is more polar.

Correlation of the Stokes shift with the four-parameter solvent scale (r^2=0.9311) reveals that the increase of solvent polarizability decreases the Stokes shift (a negative value of adjustment parameter) in opposite to the remaining three parameters. The biggest contributions to the changes of Stokes shift have solvent polarizability (41%) and solvent acidity (37%), whereas the solvent dipolarity (15%) and solvent basicity (7%) have minor influence on a Stokes shift. A good correlation of the Stokes shift was also obtained using Kamlet-Taft equation (r^2=0.9241). In this case, two parameters, solvent polarizability/polarity (41%) and solvent acidity (59%), play a crucial role. Because of a small value and large error, solvent basicity can be omitted without deterioration of the quality of fit (r^2=0.9160 whereas for original fit r^2=0.9241).

The correlation of the fluorescence quantum yield with SP, SdP, SA, SB as independent variables gives a rather good fit (r^2=0.8879, Table 2). Moreover, it indicates that all solvent parameters influence the fluorescence quantum yield. Solvent acidity (37%) and solvent dipolarity (42%) increases the fluorescence quantum yield to a similar degree, while solvent dipolarity and basicity have only a little impact on it (9% and 12%, respectively). The same conclusion arises from the Kamlet-Taft correlation (r^2=0.9306). Solvent polarizability/dipolarity and solvent acidity affect almost equally (42% and 41%, respectively) while solvent basicity in a much lesser extent (17%).

A good fit was also obtained for the fluorescence lifetime correlation with both Catalán (r^2=0.9386) and Kamlet-Taft (r^2=0.9638) equations. The largest impact on the increase of fluorescence lifetime has solvent acidity (68% and 53% for Catalán and Kamlet-Taft correlation, respectively) whereas solvent dipolarity contributes with 14% and 17%, respectively. Moreover, the contribution of solvent basicity is different for these two solvent scale. For Kamlet-Taft scale solvent basicity contribution (30%) is almost twice of that of Catalán scale (18%).

The decay of the fluorescence intensity of 3,6-di-tert-butyl-8H-indolo[3,2,1-de]acridin-8-one can be described as a mono-exponential function, except for ethyl ether solution, thus, further analysis including the dependence of fluorescence lifetime, fluorescence rate constant and radiationless rate constant on solvent polarity parameters can be performed. Analysis of the influence of the solvent on the radiative and non-radiative rate constants gives information which one depends on the solvent parameters enabling to estimate which path of the excited state deactivation predominates. The multi-linear analysis of k_f according to eq. (6) and (7) revealed that it does not correlate with solvent parameters (r^2=0.4389 for Catalán and r^2=0.4070 for Kamlet-Taft correlation, respectively) (Tables 2 and 3), however, it depends exclusively on solvent polarizability/polarity. In contrast to k_f, non-radiative rate constant k_{nr} give good correlations (r^2=0.8987 for Catalán and r^2=0.9441 for Kamlet-Taft equation, respectively) with all adjustment coefficients negative. The larger decrease of k_{nr} is caused by solvent polarizability/polarity (44% and 50% for Catalán and Kamlet-Taft correlation, respectively), solvent acidity (36% and 23%) and solvent basicity (20% and 27%). It is worth mentioning that solvent polarizability in Catalán solvent scale has no impact on k_{nr}. Moreover, a good correlation between k_{nr} and solvent acidity parameter (α and SA) for alcohols were found (Figs 12 ESI and 13 ESI). Thus, the invariance of k_f and dependence of k_{nr} on the solvent properties indicate that the change of the fluorescence quantum yield and the fluorescence decay time with solvent properties is mainly due to the change of the k_{nr} rate constant.

Among three different solvent polarity scales used in this work, Reichardt`s empirical one is a useful and easy to apply, but because it is a one-parameter scale, it does not reflect the complexity of solute-solvent interactions. However, it allows to easily determine whether the solvent studied shows a deviation from linearity due to specific interactions. Its additional advantage is possibility to estimate the dipole moment change in the excited state based on the Stokes shift dependence on E_T^N. Another two solvent polarity scales are more useful as they are multi-parametric. They allow to estimate the impact of various solvent parameters on studied quantity. For this reason a four-parameter scale has advantage over the Kamlet-Taft scale because it allows to assess independently the impact of both the polarizability and dipolarity, however, both offer comparable quality of the fit. In the case of multi-parametric solvents scales, better quality of the fits are obtained than for Reichardt`s due to the greater number of variables. Thus, in order to evaluate which scale used gives a better quality of the fit, the adjusted r^2 rather than coefficient of determination (r^2) should be applied. The explanation of adjusted r^2 is almost the same as r^2 but it penalizes the statistics as extra variables included in the model.

3.4 Specific interactions

A variety of solvent interactions with solute may be responsible for the solvent effect on the properties of solute. The solvent effect can be split into two different type of interactions: specific involving charge-transfer interactions, acid-base interactions, π-π interactions and hydrogen bonding, while those interactions which arise from the solvent acting as a dielectric continuum are referred to as non-specific interactions. The classification of solvents with respect to their polarity/polarizability and hydrogen bonding ability are based on the Kamlet-Taft or Catalán solvent polarity scale. Solvents capable to form hydrogen bond have been classified as hydrogen-bond acceptors, e.g. possessing ability to accept hydrogen atom from solute (β parameter in Kamlet-Taft scale or SB parameter in Catalán scale), and hydrogen-bond donor, e.g. possessing ability to donate hydrogen atom to solute to form hydrogen bond (α parameter in Kamlet-Taft scale or SA parameter in Catalán scale). The protic solvents mostly used in solvatochromic studies have both hydrogen-donor and hydrogen-acceptor properties. In solvatochromic studies, the shift of maximum of absorption or emission spectra depends on both non-specific interactions and solute-solvent hydrogen-bonds formation.

In a series of publications, Maciejewski and co-workers[10,25-27] gave a method to extract the contribution of specific interactions between solute and hydrogen-bonding solvents based on solvatochromic data. The first step in this method requires determination of the contribution of non-specific interactions based on solvatochromic shift of absorption and emission spectra of compound studied. The solvent used for the estimation of non-specific interactions are 1-chloro-n-alkanes[10]. These solvents interact only non-specifically because they do not have π-electron, and charge-transfer character, and do not form hydrogen bond. The straight-line obtained from solvatochromic studies of solute in 1-chloro-n-alkanes describes the effect of non-specific interactions on position of maximum of absorption and emission spectra not only in these solvents but also in other solvents that make hydrogen bond. The distance between ν_{abs} or ν_{fluo} value and the straight line describes the changes in the energy of hydrogen bond in Franck-Condon excited state (from ν_{abs} dependence) or relaxed excited state (from ν_{fluo} dependence) in a given solvent according to equation (eq. 8)[10]:

$$\Delta\nu_{shift}^{abs}(H-bond)=\nu_{abs}^{\max}(f(\varepsilon,n^2))-\nu_{abs}^{\max}(\exp)$$
$$\Delta\nu_{shift}^{fluo}(H-bond)=\nu_{fluot}^{\max}(f(\varepsilon,n^2))-\nu_{fluo}^{\max}(\exp) \quad (8)$$

where: $\nu_{abs}^{\max}(\exp)$ and $\nu_{fluo}^{\max}(\exp)$ are experimental positions of the maxima of absorption and fluorescence spectra of the solute in the solvent forming the hydrogen bond, $\nu_{abs}^{\max}(f(\varepsilon,n^2))$ and $\nu_{fluo}^{\max}(f(\varepsilon,n^2))$ are the values of predicted maxima of absorption and fluorescence spectra of the solute in this solvent based on the non-specific interaction only (from straight line of solvatochromic plot) and $f(\varepsilon,n^2)$ is the orientation polarizability function. The orientation polarizability function for a spherical cavity radius can be calculated according to various formulas[11]. For a linear Stark effect and neglecting solute polarizability (α=0) the MacRae function is used (eq. 9):

$$f_{MR}(\varepsilon,n^2)=\frac{\varepsilon-1}{\varepsilon+2}-\frac{n^2-1}{n^2+2} \quad (9)$$

Solvent polarizability function for spherical cavity with the radius (a) obtained from Bilot-Kawski theory in which linear and quadratic Stark effect was taken into account and with approximation that the polarizability of the solute is equal $2\alpha/4\pi\varepsilon_0 a^3=1$ is as follows:

$$f_{BK}(\varepsilon,n^2)=\frac{2n^2+1}{n^2+2}\left(\frac{\varepsilon-1}{\varepsilon+2}-\frac{n^2-1}{n^2+2}\right) \quad (10)$$

If the polarizability of the solute is neglected (α=0), Lippert-Mataga in the form below is used:

$$f_{LM}(\varepsilon,n^2)=\frac{\varepsilon-1}{2\varepsilon+1}-\frac{n^2-1}{2n^2+1} \quad (11)$$

In the papers published by Maciejewski et al.[10,25-27] dedicated to the calculation of energy changes of hydrogen bonds in the excited state, the Lippert-Mataga polarizability function was used. We decided to use the Bilot-Kawski polarizability function. It is worth noting that the function selection has practically no effect on the calculated values of the hydrogen bond energy changes, however, Bilot-Kawski function has a wider range of changes, which allows a more accurate approximation of nonspecific interactions by a linear approximation. The calculated changes of energy of hydrogen bond after excitation to excited (locally excited Franck-Condon and relaxed) state of 3,6-di-tert-butyl-8H-indolo[3,2,1-de]acridin-8-one in five used alcohols are presented in Table 4 and Figs 6 and 7. As can be seen from aforementioned figures a good correlation were obtained for the dependence of $\nu_{abs}^{\max}$ and $\nu_{fluo}^{\max}$ *versus* solvent polarizability function. The low value of the slop of $\nu_{abs}^{\max}$ *vs.* $f_{BK}(\varepsilon,n^2)$ indicates that the dipole moment of compound studied is nearly the same in S_0 and S_1^{FC} state, however, in the relaxed excited state the dipole moment increases (higher negative slope of the dependence of $\nu_{fluo}^{\max}$ *vs.* $f_{BK}(\varepsilon,n^2)$). Also, like for coumarins[24], blue shift is observed for saturated hydrocarbons in both absorption and emission spectra. The deviation of these points from the line formed by 1-chloro-n-alkanes corresponds to the energy of interactions between permanent dipole moment of 1-chloro-n-alkane solvents and permanent and induced dipole moment of 3,6-di-tert-butyl-8H-indolo[3,2,1-de]acridin-8-one, while saturated hydrocarbon solvents can interact only through dispersion interaction[26].

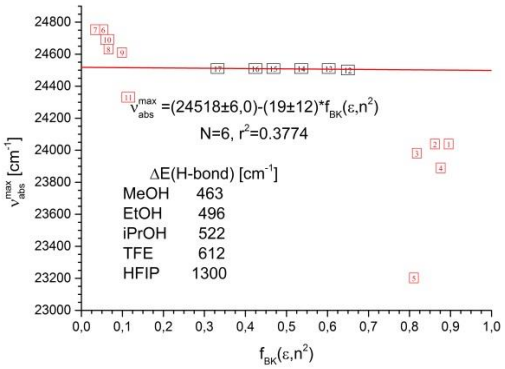

Fig. 6 The solvatochromic plot of the $\nu_{abs}^{\max}$ dependence on Bilot-Kawski polarizability function $f_{BK}(\varepsilon,n^2)$ in: (1) MeOH, (2) EtOH, (3) iPrOH, (4) TFE, (5) HFIP, (6) hexane, (7) iso-octane, (8) hexadecane, (9) squalene, (10) cyclohexane, (11) toluene (12) 1-chloro-propane, (13) 1-chloro-butane, (14) 1-chlorohexane, (15) 1-chloro-octane, (16) 1-chloro-decane, (17) 1-chlorohexadecane. The correlation equation as well as the hydrogen bond energy changes in locally excited Franck-Condon state for alcohols studied are also shown.

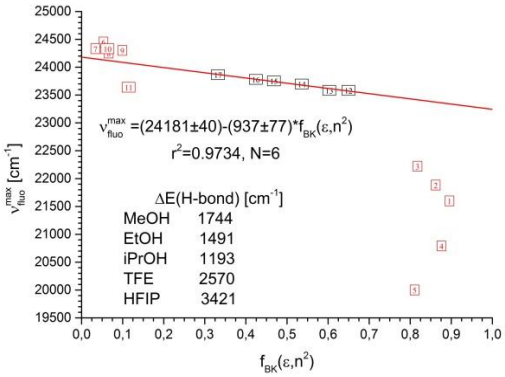

Fig. 7 The solvatochromic plot of the $\nu_{fluo}^{\max}$ dependence on Bilot-Kawski polarizability function $f_{BK}(\varepsilon,n^2)$ in: (1) MeOH, (2) EtOH, (3) iPrOH, (4) TFE, (5) HFIP, (6) hexane, (7) iso-octane, (8) hexadecane, (9) squalene, (10) cyclohexane, (11) toluene (12) 1-chloro-propane, (13) 1-chloro-butane, (14) 1-chlorohexane, (15) 1-chloro-octane, (16) 1-chloro-decane, (17) 1-chlorohexadecane. The correlation equation as well as the hydrogen bond energy changes in relaxed excited state for alcohols studied are also shown.

Moreover, red shift of absorption and emission spectrum observed for toluene can results from interactions with permanent dipole moment of solvent, however, the staking interaction with solute cannot be excluded. Because of that, in the correlation of spectroscopic properties with solvent polarizability function only 1-chloro-n-alkanes were taken into account. Moreover, the maxima of absorption and fluorescence spectra measured in alcohols are below the line defined by 1-chloro-n-alkanes which determines the non-specific interactions. Thus, the energy of hydrogen bond increases in the excited state in such a way that in the relaxed excited state the hydrogen bond is about three times stronger than that in the

locally excited Franck-Condon state (Table 4). Additionally, the changes of hydrogen bond energy follow the Kamlet-Taft or Catalán solvent acidity parameter (α or SA) (Figs 8 and 9), while the quality of fit is better for the relaxed excited state (a larger changes in the position of emission spectra) than for the locally excited Franck-Condon state.

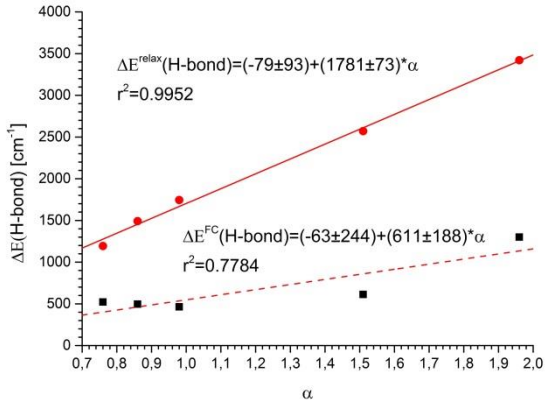

Fig. 8 The hydrogen bond energy changes in locally excited Franck-Condon excited state (dashed line) and relaxed excited state (solid line) as a function of Kamlet-Taft solvent acidity parameter (α).

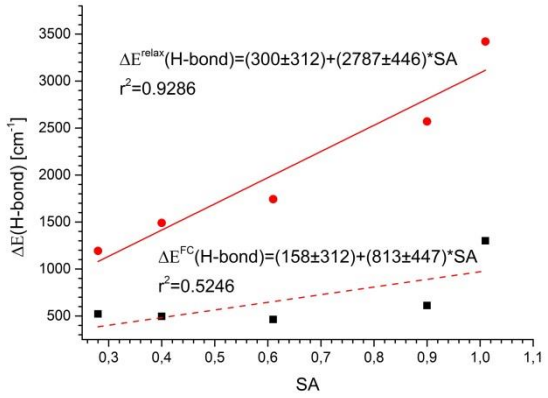

Fig. 9 The hydrogen bond energy changes in locally excited Franck-Condon excited state (dashed line) and relaxed excited state (solid line) as a function of Catalán solvent acidity parameter (SA).

Moreover, the quality of fit is better using Kamlet-Taft solvent acidity parameter (α) than Catalán parameter (SA). 3,6-Di-tert-butyl-8H-indolo[3,2,1-de]acridin-8-one can form two types of hydrogen bonds. One with lone-pair of nitrogen atom and two hydrogen bonds with lone-pairs of oxygen atom. In the excited state intramolecular charge transfer from the amino group to the carbonyl group occurs. This results in a change of the dipole moment as well as the change in the energy of hydrogen bonds. A hydrogen bond formed by a lone pair of nitrogen atom is weakened whereas those formed by a carbonyl group strengthens. After solvent relaxation, the strength of hydrogen bond formed by oxygen atom increases and simultaneously increases the dipole moment in the relaxed excited state. A smaller bathochromic shift of absorption spectra compared to the emission spectra indicates that dipole moment in the excited Franck-Condon state is smaller than in the relaxed excited state.

3.5 Calculations of dipole moment in excited state

According to Bilot-Kawski theory[18-21], the change of dipole moment in the excited state can be calculated, basing on the spectroscopic data, from following equations:

$$\tilde{\nu}_{abs}^{max} - \tilde{\nu}_{fluo}^{max} = m_1 f_{BK}(\varepsilon, n^2) + const$$
$$\tilde{\nu}_{abs}^{max} + \tilde{\nu}_{fluo}^{max} = -m_2[f_{BK}(\varepsilon, n^2) + 2g(n)] + const \quad (12)$$

where $f(\varepsilon,n^2)$ is given by eq. (9) while

$$g(n) = \frac{3(n^4-1)}{2(n^2+2)^2} \quad (13).$$

Using a slope obtained from eq. (12) and knowing the ground state dipole moment (μ_g), the excited state dipole moment can be calculated using equation,

$$\mu_e = \sqrt{\mu_g^2 + m_2 \beta a^3} \quad (14)$$

where: *a* is Onsager`s interaction radius of the solute and $\beta=2\pi\varepsilon_0 hc=1.10511044x10^{-35}$ C^2 is the universal constant. If ground and excited state dipole moments are not parallel, an angle ψ between them can be calculated according to equation (15):

$$\cos\varphi = \frac{1}{2\mu_g\mu_e}[(\mu_g^2+\mu_e^2) - \frac{m_1}{m_2}(\mu_e^2-\mu_g^2)] \quad (15)$$

To calculate the excited state dipole moment, the ground state dipole moment is necessary. It was obtained from theoretical calculation performed applying DFT method with a def2-TZVP basis set (TURBOMOLE v. 6.1) and is equal to μ_g=4.32 D. The calculation of excited state dipole moment value was performed taking into account only saturated hydrocarbons and 1-chloro-n-alkanes. The correlation of spectral properties with Bilot-Kawski solvent polarizability functions according to eq. (12) are satisfactory (r^2=0.9623, m_1=1063 cm^{-1} and r^2=0.9853, m_2=1763 cm^{-1}, respectively) (Figs 14 ESI and 15 ESI). The calculated excited state dipole moment using Onsager`s cavity radius equal to a=6.63 Å is equal to μ_e=8.35 D whereas an angle between the ground and excited state dipole moment is 36^0. Thus, the excited state dipole moment is about two times larger than in the ground state. Apart from the rigid structure of 3,6-di-tert-butyl-8H-indolo[3,2,1-de]acridin-8-one a meaningful change of the angle between ground and excited state dipole moments is observed indicating on the substantial modification of charge distribution in the relaxed excited state. As mentioned above, the excited state dipole moment was calculated taking into account saturated hydrocarbons and 1-chloro-n-alkanes only. In Figs 14 ESI and 15 ESI, the best fit to the equations (12) considering all solvents except alcohols (dashed line) are also shown. The quality of fit is of course worse, however, the slope differs only slightly from the value of slope obtained for saturated and 1-chloro-n-hydrocarbons resulting in a small change of the calculated dipole moment compared to that calculated for saturated and 1-chloro-hydrocarbons solvents. The solvatochromic plot of ν_{abs}^{max} and ν_{fluo}^{max} *versus* $f_{BK}(\varepsilon,n^2)$ for all studied solvents are shown in Fig. 16 ESI. Omitting the data for alcohols, it should be noted that

the largest deviation from linearity is observed for solvents with a quadrupole moment and with a single bond dipole moment, and for solvents with bond dipole centered at a single atom. These solvents appear more polar locally to optical probe molecule than expected on the basis of bulk dielectric constant [39]. The correlation of the Stokes shift with the microscopic solvent polarity parameter E_T^N can be applied to calculate the dipole moment change between the excited and ground state. According to the equation proposed by Ravi et al.[40] and Kumar at al.[41], the problem associated with the Onsager`s radius estimation can be minimized since a ratio of two Onsager`s radii is involved according to equation (16):

$$\nu_{abs}^{\max} - \nu_{fluo}^{\max} = 11307.6\left[\left(\frac{\Delta\mu}{\Delta\mu_B}\right)^2\left(\frac{a_B}{a}\right)^3\right]E_T^N + const \quad (16)$$

where $\Delta\mu_B$ and a_B are the dipole moment change ($\Delta\mu=\mu_e-\mu_g$) and Onsager's radius, respectively, for a pyridinium N-phenolate betaine dye used to determine the E_T^N values ($\Delta\mu_B$=9 D and a_B=6.2 Å), whereas $\Delta\mu$ and a are the corresponding quantities for the molecule under study. The slope of dependence of Stokes shift *vs*. E_T^N parameter is equal to 2736 (Fig. 3 ESI) which according to equation (16) gives $\Delta\mu$=4.8 D and thereby μ_e=9.1 D. This value is larger than that calculated basing on Bilot-Kawski theory, however, in calculation according to eq (16) all solvents studied were used including alcohols.

Conclusions

The observed solvatochromism of 3,6-di-tert-butyl-8H-indolo[3,2,1-de]acridin-8-one is a result of the increase of the excited state dipole moment. Therefore the solvent-dependent spectroscopic and photophysical properties were analyzed using the Reichard's as well as Kamlet-Taft and Catalán solvent scales. The analysis of these relationships leads to the conclusion that the solvent polarity and solvent hydrogen-bonding donor ability have major influence on measured values. The radiationless deactivation rate constant value decreases with a decrease of the $\Delta E(S_1\text{-}S_0)$ energy gap not only for molecule but also for hydrogen-bonded complex. It means that the increase of solvent polarity causes the decrease of S_1-T intersystem rate constant and thereby decreases the intersystem crossing which seems to be the main route of deactivation of the excited state.

Additionally, the spectroscopic properties of this compound were investigated in protic and non-protic solvents and the results were discussed in terms of hydrogen-bonding. It was experimentally found that 3,6-di-tert-butyl-8H-indolo[3,2,1-de]acridin-8-one forms hydrogen bonds which are overall strengthened in the locally excited Franck-Condon and relaxed excited states compared to that of the ground state.

Acknowledgements

This work was financially supported by the grant for Young Scientists No. 538-8443-B046-13 from the University of Gdańsk.

Notes and references

Faculty of Chemistry, University of Gdańsk
Wita Stwosza 63, 80-308 Gdańsk, Poland
* corresponding author, e-mail wieslaw.wiczk@ug.edu.pl

† Electronic Supplementary Information (ESI) available: [includes correlations of spectral and photophysical parameters with Reichardt`s solvent polarity parameter E_T^N, luminescence spectra at 77 K as well as the correlation of the difference and the sum of absorption and emission maxima *versus* Bilot-Kawski polarity functions]. See DOI: 10.1039/b000000x/

1 P. Belmont, J. Bosson, T. Godet, M. Tiano, *Anticancer Agents Med.Chem*., 2007, **7**, 139.
2 G. Cholewiński, K. Dzierzbicka, A. M. Kołodziejczyk, *Pharmacol Rep*., 2011, **63**, 305.
3 A. F. Valdés, *Open Med. Chem.,*2011, **5**, 11.
4 P. Yang, Q. Yang, L. Tong, X. Li, *J. Photochem. Photobiol. B:Biol.,* 2006, 84, 221.
5 Y. Hagivara, T. Hasegawa, A. Shoji, M. Kuwahara, H. Ozaki, H. Sawai, *Bioorg. Med. Chem*., 2008, **16**, 7013.
6 C. Gao, S. Li, X. Lang, H. Liu, F. Liu, C. tan, Y. Jiang, *Tetrahedron*, 2012, **68**, 7920.
7 B. Qiu, L. Guo, Z. Chen, Y. Chi, L. Zhang, G. Chen, *Biosens. Bioelectron*., 2009, **24**, 1281.
8 S. Cosnier, P. Mailley, *Analyst*, 2008, **133**, 984.
9 P. Suppan, N. Ghoneim, Solvatochromism, The Royal Society of Chemistry, Cambridge, U.K., 1997.
10 E. Krystkowiak, K. Dobek, A. Maciejewski, *J. Photochem. Photobiol. A:Chem.,* 2006, **184**, 250.
11 G.-J. Zhao, K.-L. Han, *Acc. Chem. Res*., 2012, **45**, 404.
12 K. Guzow, M. Milewska, W. Wiczk, *Spectrochim. Acta A*, 2005, **61**, 1133.
13 K. Guzow, A. Ceszlak, M. Kozarzewska, W. Wiczk, *Photochem. Photobiol. Sci.,* 2011, **10**, 1610.
14 K. Guzow, M. Czerwińska, A. Ceszlak, M. Kozarzewska, M. Szabelski, C. Czaplewski, A. Łukaszewicz, A. A. Kubicki, W. Wiczk, *Photochem. Photobiol. Sci.,* 2013, **12**, 284.
15 A. Filarowski, M. Kluba, K. Cieślik-Boczula, A. Koll, A. Kochel, L. Pandey, W. M. De Borggrave, M. van der Auweraer, J. Catalán, N. Boens*, Photochem. Photobiol. Sci*., 2011, **9**, 996.
16 C. Reichardt, *Chem. Rev*., 1994, **94**, 2319.
17 C. Reichardt, E. Harbusch-Görnert, *Liebigs Ann. Chem*., 1983, 721.
18 A. Kawski, in: J. F. Rabek (Ed.), Progress in Photochemistry and Photophysics, vol. 5, CRC Press, Boca Raton, USA, 1992, pp. 1–47.
19 A. Kawski, P. Bojarski, in: P. R. Somani (Ed.), Chromic Materials, Phenomena and Their Technological Applications, Applied Science Innovations, 2009, pp. 114-163.
20 L. Bilot, A. Kawski, *Naturforsch.* 1962, **17a**, 621.
21 L. Bilot, A. Kawski, *Naturforsch.* 1963, **18a**, 10 and 256.
22 M. J. Kamlet, J.-L. M. Abboud, R. W. Taft, *Prog. Phys. Org. Chem*., 1982, **13**, 485.
23 J. Catalán, *J. Phys. Chem. B*, **113** (2009) 5951.
24 W. Zhao, L. Pang, W. Bian, J. Wang, *ChemPhysChem*, 2008, **9**, 1593.
25 E. Krystkowiak, K. Dobek, A. Maciejewski, *Photochem. Photobiol. Sci*., 2013, **12**, 446.
16 E. Krystkowiak, K. Dobek, G. Burdziński, A. Maciejewski, *Photochem. Photobiol. Sci*., 2012, **11**, 1322.
27 E. Krystkowiak, A. Maciejewski, *Phys. Chem. Chem. Phys*., 2011, **13**, 11317.
28 F. C. Chipen, A. Mishra, G. Krishnamoorthy, *Phys. Chem. Chem. Phys*., 2012, **14**, 8775.
29 Y. Liu, M. Nishiura, Y. Wang, Z. Hou, *J. Am. Chem. Soc*., 2006, **128**, 5592.

30 M. V. Skorobogatyi, A. A. Pchelintseva, A. L. Petrunina, I. A. Stepanova, V. L. Andronova, G. A. Galegov, A. D. Malakhov, V. A. Korshun, *Tetrahedron*, 2006, **62**, 1279.
31 J. R. Lakowicz, Principles of Fluorescence Spectroscopy, 2nd ed., Kluwer Academic/Plenum Publishers, New York, 1999.
32 M. Baruah, W. Qin, C. Flores, J. Hofkens, R. A. L. Valle, D. Beljonne, M. Van der Auweraer, W. M. De Borggrave, N. Boens, *J. Phys. Chem. A,* 2006, **110**, 5998.
33 J. Jayabarathi, V. Thanikachalam, K. Jayamoorthy, *Photochem. Photobiol. Sci*., 2013, **121,** 761.
34 R. Englman, J. Jortner, M*ol. Phys.,*1970, **18**, 145.
35 Postgraduate Chemistry Series. Photochemistry of Organic Compounds. From Concept to Practice, P. Klán, J. Wirz, J. Wiley & Sons Lt., 2009, UK
36 N. J. Turro, V. Ramamuthry, J. C. Scaiano, Principles of Molecular Photochemistry. An Introduction, Chapter 5, University Science Book, Sausalito, California, 2009.
37 R. Lopez-Artega, A. B. Stephansen, C.A. Guarin, T.I. Solling, J. Peon, *J. Phys. Chem. B,* 2013, **117**, 9947.
38 X. Liu, J.M. Cole, K.S. Low, *J. Phys. Chem. C*, 2013, **117**, 14731.
39 I. Renge, *J. Phys. Chem. A*, 2010, **114**, 6250.
40 M. Ravi, A. Samanta, T. P. Radharkrishnan *J. Phys. Chem. A*, 1994, **98**, 9133.
41 S. Kumar, V.C. Rao, R. C. Rostogi, *Spectrochim. Acta*, *Part A*, 2001, **57**, 41.

Journal Name RSCPublishing

ARTICLE

Table 1. Spectroscopic and photophysical properties of 3,6-di-tert-butyl-8H-indolo[3,2,1-de]acridin-8-one in solvents used.

nr	Solvent	ν_{abs} [cm^{-1}]	ν_{em} [cm-1]	$\Delta\nu$ [cm^{-1}]	φ	τ [ns]	k_f*10^{-7} [s^{-1}]	$k_{nr}*10^{-7}$ [s^{-1}]
1	MeOH	24038	21598	2440	0.469	5.71	8.28	9.30
2	EtOH	24038	21882	2156	0.445	5.20	8.56	10.67
3	iPrOH	23981	22222	1759	0.396	4.59	8.64	13.15
4	TFE	23889	20790	3019	0.532	6.09	8.73	7.69
5	HFiP	23202	20000	3202	0.689	6.69	10.30	4.65
6	Hexane	24752	24450	302	0.010	0.98	0.98	101.06
7	Isooctane	24752	24331	421	0.010	0.98	1.04	101.00
8	Hexadecane	24630	24253	277	0.034	0.85	4.02	113.62
9	Squalene	24610	24301	309	0.047	0.82	5.79	116.16
10	Cyclohexane	24691	24331	360	0.010	0.91	1.11	108.78
11	Toluen	24331	23640	691	0.251	1.12	22.42	66.87
12	1-chloropropane	24501	23584	926	0.164	1.47	11.14	56.89
13	1-chlorobutane	24510	23584	926	0.127	1.37	9.29	63.70
1`4	1-chlorohexane	24510	23697	813	0.112	1.11	10.09	80.00
15	1-chlorooctane	24510	23753	757	0.103	1.07	9.59	83.87
16	1-chlorodecane	24510	23780	730	0.056	0.96	5.85	98.31
17	1-chlorohexadecane	24510	23864	646	0.034	0.78	4.38	123.82
18	Acetone	24390	23148	1242	0.226	2.28	9.92	33.94
19	Acetonitrile	24331	22831	1500	0.253	3.21	7.87	23.29
20	Dioxane	24450	23364	1086	0.229	1.52	15.06	50.73
21	THF	24450	23640	810	0.149	1.35	11.04	63.03
22	MeTHF	24510	23471	1039	0.134	1.17	11.48	73.99
23	Et_2O	24630	23302	1328	0.272	0.36 (α=0.46) 1.44 (α=0.54)	--	--
24	AcOEt	24510	23584	926	0.134	1.41	9.48	61.44
25	DMF	24272	22831	1441	0.325	2.91	11.18	23.18
26	DMSO	24096	23256	840	0.388	3.38	11.49	18.10

Table 2 Estimated coefficients (y_0, a_{SP}, b_{SdP}, c_{SB}, d_{SA}), their errors and correlation coefficients (r^2) for multi-linear correlation analysis of ν_{abs}, ν_{fluo}, φ, τ, $\Delta\nu$, k_f, k_{nr} of compound as a function of the Catalán four-parameter solvent scale (eq. 7).

	y_0	a_{SP}	b_{SdP}	c_{SB}	d_{SA}	r^2	N
ν_{abs} [cm^{-1}]	25601±257	-(1355±376)	-(229±84)	-(172±109)	-(873±119)	0.9190	20
ν_{fluo}	23836±743	608±1087	-(973±243)	-(450±316)	-(2711±343)	0.9510	20
[cm^{-1}]	24248±101	-	-(945±232)	-(451±309)	-(2711±343)	0.9500	
$\Delta\nu$ [cm^{-1}]	1774±668	-(2007±978)	752±218	318±284	1777±308	0.9311	20
φ	-(0.347±0.186)	0.566±0.273	0.122±0.061	0.163±0.079	0.497±0.086	0.8879	20
$\tau*10^9$	0.626±1.160	0.113±2.378	1.105±0.508	1.404±0.686	5.280±0.719	0.9368	19
[ns]	0.702±0.205	-	1.108±0.487	1.407±0.659	5.258±0.534	0.9368	
k_f*10^{-8}	-(3.020±1.382)	5.262±2.010	0.488±0.429	-(0.158±0.580)	0.616±0.607	0.4552	19
[s^{-1}]	-(2.130±0.986)	3.945±1.412	0.581±0.243	-	-	0.4389	
$k_{nr}*10^{-9}$ [s^{-1}]	1.345±0.447	-(0.426±0.652)	-(0.630±0.139)	-(0.286±0.188)	-(0.511±0.197)	0.9017	19
	1.056±0.057	-	-(0.641±0.136)	-(0.299±0.183)	-(0.429±0.149)	0.8987	

Table 3 Estimated coefficients (y_0, a_{π^*}, b_α, c_β), their errors and correlation coefficients (r^2) for multi-linear correlation analysis of ν_{abs}, ν_{fluo}, φ, τ, Δν, k_f, k_{nr} of compound as a function of the Kamlet-Taft solvent scale (eq. 6).

	y_0	a_π^*	b_α	c_β	r^2	N
ν_{abs} [cm^{-1}]	24720±50	-(491±119)	-(492±48)	-(20±107)	0.9231	20
	24718±50	-(505±90)	-(489±45)	-	0.9139	
ν_{fluo}[cm^{-1}]	22224±94	-(1122±227)	-(1758±92)	-(306±203)	0.9731	20
	24205±97	-(1334±184)	-(1719±97)	-	0.9693	
Δν [cm^{-1}]	478±113	630±272	1258±110	231±244	0.9241	20
	497±115	852±218	1216±108	-	0.9160	
φ	0.027±0.02)	0.248±0.058	0.238±0.023	0.097±0.052	0.9306	20
$\tau*10^9$ [ns]	0.764±0.188	0.944±0.454	2.917±0.177	1.683±0.403	0.9638	19
k_f*10^{-7}[s^{-1}]	3.509±1.850	15.023±4.463	-(1.812±1.735)	-(4.370±3.965)	0.4704	19
	3.321±1.834	11.103±3.251	-	-	0.4070	
$k_{nr}*10^{-8}$ [s^{-1}]	10.444±0.444	-(6.786±1.073)	-(3.110±0.417)	-(3.627±0.953)	0.9441	19

Table 4. Hydrogen bond energy changes after photoexcitation of 3,6-di-tert-butyl-8H-indolo[3,2,1-de]acridin-8-one in alcohols calculated based on solvatochromic plot of absorption and emission spectra.

solvent	ΔE(H-bond) [cm^{-1}]		Kamlet-Taft (α) and Catalan (SA) solvent H-bond donating parameter	
	S_1^{FC}	S_1^{relax}	α	SA
iPrOH	522	1193	0.76	0.28
EtOH	496	1491	0.86	0.40
MeOH	463	1744	0.98	0.61
TFE	612	2570	1.51	0.90
HFIP	1300	3421	1.96	1.01